Numerical modeling of electromagnetic coupling phenomena in the vicinities of overhead power transmission lines

Lucas Blattner Martinho

LUCAS BLATTNER MARTINHO

NUMERICAL MODELING OF ELECTROMAGNETIC COUPLING PHENOMENA IN THE VICINITIES OF OVERHEAD POWER TRANSMISSION LINES

Thesis submitted to the University of São Paulo and to the University Grenoble Alpes to meet the requirements established by their doctoral programs in Electrical Engineering.

São Paulo
2016

LUCAS BLATTNER MARTINHO

NUMERICAL MODELING OF ELECTROMAGNETIC COUPLING PHENOMENA IN THE VICINITIES OF OVERHEAD POWER TRANSMISSION LINES

Thesis submitted to the University of São Paulo and to the University Grenoble Alpes to meet the requirements established by their doctoral programs in Electrical Engineering.

Concentration Area:

Power Systems

Advisors:

Prof. Dr. Viviane Cristine Silva
Dr. Olivier Chadebec

São Paulo
2016

Catalogação-na-publicação

Martinho, Lucas Blattner
Numerical modeling of electromagnetic coupling phenomena in the vicinities of overhead power transmission lines / Lucas Blattner Martinho; orientadores Viviane Cristine Silva; Olivier Chadebec -- São Paulo/Grenoble, 2016.
117 p.

Tese (Doutorado com dupla titulação) - Escola Politécnica da Universidade de São Paulo. Departamento de Engenharia de Energia e Automação Elétricas. Université Grenoble Alpes. Laboratoire de Génie Électrique de Grenoble.

1.Linhas de transmissão em alta tensão 2.Acoplamento eletromagnético 3. Aterramento 4.Método dos elementos finitos 5.Método PEEC I.Universidade de São Paulo. Escola Politécnica. Departamento de Engenharia de Energia e Automação Elétricas II.Université Grenoble Alpes. Laboratoire de Génie Électrique de Grenoble. III.t.

Communauté
UNIVERSITÉ Grenoble Alpes

Universidade de São Paulo

THÈSE

Pour obtenir le grade de

DOCTEUR DE L'UNIVERSITÉ GRENOBLE ALPES

préparée dans le cadre d'une cotutelle entre l'Université Grenoble Alpes et l'Université de São Paulo

Spécialité : **Génie Électrique**

Arrêté ministériel : le 6 janvier 2005 - 7 août 2006

Présentée par

Lucas BLATTNER MARTINHO

Thèse dirigée par **Olivier CHADEBEC** et **Viviane Cristine SILVA** et codirigée par **Gérard MEUNIER**

préparée au sein du **Laboratoire de Génie Électrique de Grenoble** et de **l'École Polytechnique de l'Université de São Paulo**

dans les Écoles Doctorales **EEATS (Electronique, Electrotechnique, Automatique & Traitement du Signal)** et **PPGEE (*Programa de Pós-Graduação em Engenharia Elétrica*)**

Modélisation numérique des phénomènes de couplage électromagnétique dans les alentours des lignes aériennes de transmission d'énergie

Thèse soutenue publiquement le **23/03/2016**, devant le jury composé de :

M. João Pedro ASSUMPÇÃO BASTOS
Professeur de l'Université Fédérale de Santa Catarina (Brésil), Président et Rapporteur
M. Laurent KRÄHENBÜHL
Directeur de recherche au CNRS (France), Rapporteur
M. Renato CARDOSO MESQUITA
Professeur de l'Université Fédérale de Minas Gerais (Brésil), Membre
M. Olivier CHADEBEC
Directeur de recherche au CNRS (France), Membre
M^me^ Viviane Cristine SILVA
Professeur de l'Université de São Paulo (Brésil), Membre
M. Gérard MEUNIER
Directeur de recherche au CNRS (France), Invité

ACKNOWLEDGEMENTS

I would like to express my sincere gratitude to Prof. Dr. Viviane Cristine Silva, my advisor at the University of São Paulo (USP), for her prompt guidance in the course of this research and for the many years of trustful collaboration. In the same way, I would like to express my very great appreciation to Dr. Olivier Chadebec and Dr. Gérard Meunier, my advisors from the University Grenoble Alpes (UGA), for the warm welcome granted to me in France and for their invaluable guidance along the period we worked together.

This thesis was conducted in the context of a double degree program involving the USP and the UGA. With regard to the establishment of this cooperation between the two universities, I must also thank my advisors of both institutions for their diligent efforts. Prof. Dr. Luiz Lebensztajn and Prof. Dr. José Roberto Cardoso from the USP also dedicated their attentions to the settlement of this agreement, and the assistance they provided in these matters was greatly appreciated.

My grateful thanks are also extended to Dr. Mario Leite Pereira Filho, who introduced me to the subject of this thesis during my attachment to the Institute of Technological Research of the State of São Paulo (IPT - *Instituto de Pesquisas Tecnológicas*). Additionally, Dr. Mario Leite provided me with some of the illustrations in chapter 1 and with comparative results yielded by the Method of Complex Images occurring in chapter 4, for which I am also very grateful.

I would like to acknowledge Dr. Marcelo Facio Palin and Dr. Sérgio Luís Lopes Verardi as well, who aided me with implementation aspects in the finite

element analysis of conductive coupling problems in the earliest periods of the research. Similarly, I am much obliged to the cooperation of Dr. Bertrand Bannwarth, Dr. Jean-Michel Guichon, Dr. Thanh Trung Nguyen and Mr. Jonathan Siau, who helped me with software implementation issues related to the generalized Partial Element Equivalent Circuit Method during my later period in France.

Mrs. Cristina Borba scrutinized the preliminary versions of this document and enlightened me with numerous corrections in the use of the English language. I would like to thank her for her careful reading of the manuscript, which greatly collaborated on its improvement.

The research corresponding to this work was supported by the State of São Paulo Research Foundation (FAPESP - *Fundação de Amparo à Pesquisa do Estado de São Paulo*), who conferred me grants 2011/03450-1 and 2013/21888-0 and to whom I would like to show my gratefulness.

Finally, I would like to thank my fellow labmates, friends and family for the continued support of this endeavor throughout the previous years.

São Paulo, January 2016.

Les minutes, mortel folâtre, sont des gangues
Qu'il ne faut pas lâcher sans en extraire l'or !

Souviens-toi que le Temps est un joueur avide
Qui gagne sans tricher, à tout coup ! c'est la loi.

L'Horloge, Charles BAUDELAIRE.

ABSTRACT

MARTINHO, L. B. *Numerical modeling of electromagnetic coupling phenomena in the vicinities of overhead power transmission lines*. 117 p. Thesis (PhD) — Universidade de São Paulo and Université Grenoble Alpes, 2016.

Electromagnetic coupling phenomena between overhead power transmission lines and other nearby structures are inevitable, especially in densely populated areas. The undesired effects resulting from this proximity are manifold and range from the establishment of hazardous potentials to the outbreak of alternate current corrosion phenomena. The study of this class of problems is necessary for ensuring security in the vicinities of the interaction zone and also to preserve the integrity of the equipment and of the devices there present. However, the complete modeling of this type of application requires the three-dimensional representation of the region of interest and needs specific numerical methods for field computation. In this work, the modeling of problems arising from the flow of electrical currents in the ground (the so-called conductive coupling) will be addressed with the finite element method. Those resulting from the time variation of the electromagnetic fields (the so-called inductive coupling) will be considered as well, and they will be treated with the generalized PEEC (Partial Element Equivalent Circuit) method. More specifically, a special boundary condition on the electric potential is proposed for truncating the computational domain in the finite element analysis of conductive coupling problems, and a complete PEEC formulation for modeling inductive coupling problems is presented. Test configurations of increasing complexities are considered for validating the foregoing approaches. These works aim to provide a contribution to the modeling of this class of problems, which tend to become common with the expansion of power grids.

Keywords: High-voltage transmission lines. Electromagnetic coupling. Grounding. Finite Element Method (FEM). Partial Element Equivalent Circuit (PEEC) Method.

RÉSUMÉ

MARTINHO, L. B. *Modélisation numérique des phénomènes de couplage électromagnétique dans les alentours des lignes aériennes de transmission d'énergie*. 117 p. Thèse (Doctorat) — Universidade de São Paulo et Université Grenoble Alpes, 2016. En anglais.

Les phénomènes de couplage électromagnétique entre les lignes aériennes de transmission d'énergie et des structures voisines sont inévitables, surtout dans les zones densément peuplées. Les effets indésirables découlants de cette proximité sont variés, allant de l'établissement des tensions dangereuses à l'apparition de phénomènes de corrosion dus au courant alternatif. L'étude de cette classe de problèmes est nécessaire pour assurer la sécurité dans les alentours de la zone d'interaction et aussi pour préserver l'intégrité des équipements et des dispositifs présents. Cependant, la modélisation complète de ce type d'application implique la représentation tridimensionnelle de la région d'intérêt et nécessite des méthodes numériques de calcul de champs spécifiques. Dans ces travaux, des problèmes liés à la circulation de courants électriques dans le sol (ou de couplage dit conductif) seront abordés avec la méthode des éléments finis. D'autres problèmes résultants de la variation temporelle des champs électromagnétiques (ou de couplage dit inductif) seront aussi considérés et traités avec la méthode PEEC (*Partial Element Equivalent Circuit*) généralisée. Plus précisément, une condition limite particulière sur le potentiel électrique est proposée pour tronquer le domaine de calcul dans l'analyse par éléments finis des problèmes de couplage conductif et une formulation PEEC complète pour la modélisation de problèmes de couplage inductif est présentée. Des configurations tests de complexités croissantes sont considérées pour valider les approches précédentes. Ces travaux visent ainsi à apporter une contribution à la modélisation de cette classe de problèmes, qui tendent à devenir communs avec l'expansion des réseaux électriques.

Mots-clefs : Lignes électriques à haute tension. Couplage électromagnétique. Prise de terre. Méthode des éléments finis (MEF). Méthode PEEC (*Partial element equivalent circuit*).

RESUMO

MARTINHO, L. B. *Modelagem numérica de fenômenos de acoplamento eletromagnético nas imediações de linhas aéreas de transmissão de energia*. 117 p. Tese (Doutorado) — Universidade de São Paulo e Université Grenoble Alpes, 2016. Em inglês.

Fenômenos de acoplamento eletromagnético entre linhas aéreas de transmissão de energia e outras estruturas vizinhas são inevitáveis, sobretudo em áreas densamente povoadas. Os efeitos indesejados decorrentes desta proximidade são variados, indo desde o estabelecimento de potenciais perigosos até o surgimento de processos de corrosão por corrente alternada. O estudo desta classe de problemas é necessária para a garantia da segurança nas imediações da zona de interação e também para se preservar a integridade de equipamentos e dispositivos ali presentes. Entretanto, a modelagem completa deste tipo de aplicação requer a representação tridimensional da região de interesse e necessita de métodos numéricos de cálculo de campos específicos. Neste trabalho, serão abordadas as modelagens de problemas decorrentes da circulação de correntes elétricas no solo (ditos de acoplamento condutivo) com o método dos elementos finitos. Também serão considerados problemas produzidos pela variação temporal dos campos eletromagnéticos (ditos de acoplamento indutivo), que serão tratados com o método PEEC (*Partial Element Equivalent Circuit*) generalizado. Mais especificamente, uma condição de contorno particular sobre o potencial elétrico é proposta para o truncamento do domínio de cálculo na análise de problemas de acoplamento condutivo com o método dos elementos finitos, e uma formulação completa tipo PEEC para a modelagem de problemas de acoplamento indutivo é apresentada. Problemas teste de complexidades crescentes são considerados para a validação das abordagens precedentes. Estes trabalhos visam fornecer desta forma uma contribuição à modelagem desta classe de problemas, que tendem a se tornar comuns com a expansão das redes elétricas.

Palavras-chave: Linhas de transmissão em alta tensão. Acoplamento eletromagnético. Aterramento. Método dos elementos finitos (MEF). Método PEEC (*Partial Element Equivalent Circuit Method*).

LIST OF FIGURES

LIST OF TABLES

LIST OF SYMBOLS

$\mathbf{A}$	Magnetic vector potential (Wb/m).
a_i^e	i-th edge degree of freedom of element e.
$\mathbf{B}$	Magnetic flux density vector (T).
$\mathbf{D}$	Electric displacement vector (C/m^2).
D	Geometric distance (m).
d	Geometric distance (m).
$\mathbf{E}$	Electric field (V/m).
f	Frequency (Hz).
$\mathbf{H}$	Magnetic intensity vector (A/m).
H	Geometric distance (m).
$H_n^{(1)}$	Hankel functions of the first kind and order n.
$H_n^{(2)}$	Hankel functions of the second kind and order n.
h	Geometric distance (m).
I, I_k	Electric current (A).
$[I]$	Vector of branch currents (A).
$\mathbf{J}$	Current density vector (A/m^2).
J_n	Bessel function of the first kind and order n.
j	Imaginary unit, $j = \sqrt{-1}$.
$[L]$	Inductance matrix (H).

ℓ	Electrode length or geometric distance (m).
N_i^e	i-th nodal scalar shape function from element e.
$\mathbf{n}$	Normal unit vector.
$O(n^2)$	Big O notation for quadratic complexity.
P	Point.
$\mathbf{R}$	Vector residual.
R	Electrode radius or geometrical parameter (m).
$[R]$	Resistance matrix (Ω).
$\mathcal{R}_i$	i-th weighted residual.
$\mathbf{r}$	Position vector (m).
r	Geometrical distance (m).
$\mathbf{u}$	1-D zero order shape function.
$\mathbf{v}$	Facet vector shape function.
$\mathbf{w}$	Facet vector shape function.
x	Cartesian coordinate (m).
y	Cartesian coordinate (m).
$[Z]$	Impedance matrix (Ω).
z	Cartesian coordinate or axial coordinate of a cylindrical system of coordinates (m).
Γ	Domain boundary surface.
Γ_i^e	i-th facet of element e.
$[\Delta\varphi]$	Vector of branch voltage drops (V).

δ	Skin depth (m).
δ_{ij}	Kronecker's delta; $\delta_{ij} = 1$ if $i = j$, $\delta_{ij} = 0$ if $i \neq j$.
ε	Electric permittivity (F/m).
μ	Magnetic permeability (H/m).
μ_0	Magnetic permeability of free space, $\mu_0 = 4\pi \times 10^{-7}$ H/m.
ν	Magnetic reluctivity (m/H).
ρ	Electric resistivity (Ω.m) or radial coordinate of a cylindrical system of coordinates (m).
ρ_V	Volume electric charge density (C/m^3).
σ	Electric conductivity (S/m).
$\dot{\sigma}$	Complex conductivity (S/m), $\dot{\sigma} = \sigma + j\omega\varepsilon$.
φ	Electric scalar potential (V).
φ_i^e	i-th nodal degree of freedom of element e.
Ω	Volume domain or ohm, the SI unit of electrical resistance.
ω	Angular frequency (rad/s), $\omega = 2\pi f$.
$\boldsymbol{\omega}_i^e$	i-th edge vector shape function from element e.

LIST OF ABBREVIATIONS AND ACRONYMS

AC	Alternate current.
ACSR	Aluminium conductor steel-reinforced.
BiCGStab	Biconjugate gradient stabilized method.
FEM	Finite element method.
HCA	Hybrid cross approximation.
MCI	Method of complex images.
NHDBC	Non-homogeneous Dirichlet boundary condition.
PEEC	Partial element equivalent circuit.
ZIE	Zienkiewicz infinite element.

CONTENTS

1 INTRODUCTION

1.1 Presentation

The analysis of the electromagnetic coupling between an electric power system and other nearby structures is a complex problem in electrical engineering. Even though the physical phenomena taking part in this interaction may be stated in terms of well-known electromagnetic effects, the practical situations of interest tend to be elaborate.

For instance, a typical scenario of investigation would correspond to a relatively narrow strip of land in which a long overhead power line shares a restricted space with other utilities. Ordinary buildings and other urban structures could be close to the overhead line as well, especially in subtransmission and distribution circuits. Additionally, the right of way could also be approached by working personnel or by other subjects. A real example of this situation is shown in Figure 1.

In the aforementioned problems, the analyst or engineer is most frequently concerned with safety issues arising from the proximity with the transmission system. Another major interest is the investigation of the susceptibility of structures and devices to effects induced by the electromagnetic environment represented by the vicinities of the overhead line.

As a consequence of the complexities of these problems, numerical ap-

Figure 1: An overhead line in close proximity with buildings and urban structures. The small yellow pole emerging from the ground surface marks the existence of underground structures.

proaches are required in their modeling. In the most general case, objects with arbitrary shapes and relative positions would coexist with the power line in the right of way, leading to the need for a full 3-D model to well represent the interactions between them.

This work aims to contribute with the numerical modeling of the latter category of problems. In the subsequent sections, an overview of the general electromagnetic coupling problem with a power system will be provided, in order to lay the groundwork for the following chapters. The structure and organization of this document will be presented as well, together with establishing its scope

and specific objectives.

1.2 Electromagnetic coupling phenomena in power systems

The disturbances produced by the influence of a power system in its neighboring structures are often classified into three main categories, each associated to a predominant interaction.

The first group is the one associated to the effects resulting from the time-varying magnetic flux density field $\mathbf{B}$, which is produced by the electric currents flowing in the overhead conductors. These effects are conventionally named inductive coupling phenomena. According to Faraday's law of induction, the time variation of this field brings about an induced electric field $\mathbf{E}$ in the surroundings of the transmission line and an induced electric potential distribution φ. The circulation of transient currents in the line is associated to faster rates of change for $\mathbf{B}$ and tends to produce higher induced voltages as a consequence. On the other hand, the steady state operation of the transmission line leads to lower but sustained levels of induction.

Still during a transient or a fault, current components may be diverted from the power system and drained to the soil. These current injections occur by means of shield wires, metallic towers and their grounding structures, leading to an overall rise of the electric potential in the region beneath the ground surface. The associated electric field $\mathbf{E}$ and current density $\mathbf{J}$ distributions lead to interactions that constitute a second group: the category of conductive coupling phenomena.

Moreover, the sources supplying an overhead line contained in a right of way impose both a particular voltage level between its phase conductors and

Figure 2: Excavation of a shared right of way for the maintenance of a buried pipeline.

a corresponding impressed electric field $\mathbf{E}$ in their surroundings. The establishment of this time-varying electric field in the vicinities of the line may be associated to displacement currents flowing through equivalent capacitances. The effects emerging from this flow are commonly categorized as capacitive coupling phenomena.

The electric field and the rise in the electric potential due to any of the three mechanisms previously described constitute significant engineering concerns. Touch voltages produced in metallic structures by either the inductive, capacitive or conductive coupling with an overhead line may cause the flow of larger than admissible currents through the human body, exceeding the accepted thresholds of protection against electric shock. The same holds true for step voltages arising from conductive coupling effects.

Utilities and other types of equipment may also suffer direct damage from the action of inductive, conductive and capacitive coupling phenomena. Among the structures frequently sheltered in a transmission line right of way and susceptible to electromagnetic coupling phenomena are rails, pipelines (Figure 2) and other devices attached to them such as cathodic protection systems.

Figure 3: Examples of AC corrosion developed from small coating defects in pipelines. Reproduced from (REVIE, 2015) under the permission of John Wiley & Sons, Inc.

For instance, high electric potential gradients can deteriorate the protective coating of pipelines and expose their metallic bodies to oxidation. Susceptible electronic apparatus integrating cathodic protection systems may also be directly affected by intense fields. Even AC electrochemical corrosion phenomena of metallic structures may be triggered in this particular environment by the direct action of the fields induced by the overhead line (Figure 3).

Furthermore, insulating flange connections existing between two consecutive pipeline sections may be damaged by high electric fields, causing the transfer of dangerous induced potentials to far away distances. High current densities arising from the intense conductive coupling during a fault may even pierce or perforate the metallic surfaces of underground pipelines buried close

to a tower grounding system.

In any case, the quantification and the prediction of these effects require the knowledge of the intensities of the electromagnetic fields taking part in the phenomena. However, their direct determination by means of measurements is only seldom feasible. Practical complications connected to establishing a controlled measuring experiment in a live overhead line impose significant limitations on the investigation efforts in this domain.

1.3 Objectives of this work

Taking into account the scenario previously portrayed, the alternative use of computer models for numerically determining the physical quantities involved in electromagnetic coupling phenomena becomes preeminent.

Nevertheless, the numerical modeling of this class of applications is challenging. The presence of large volumes of inactive air regions, the treatment of semi-infinite domains and the difference in scale between electrodes or phase conductors and the region actually represented in the vicinities of the overhead line are all well-known modeling challenges in the domain of computational electromagnetics.

Therefore, this work aims to contribute with the numerical modeling of this class of applications. More specifically:

- The analysis of 3-D conductive coupling problems occurring in the vicinities of an overhead line with the use of the Finite Element method (FEM) will be proposed. This method has been successfully employed for analyzing grounding arrangements for computing their equivalent impedances, and will have its application extended to this broader class of problems by the use of a particular boundary condition for treating

semi-infinite soil domains.

- The analysis of 3-D inductive coupling problems with the generalized Partial Element Equivalent Circuit (PEEC) method will be proposed as well. This integral method will be adopted to circumvent some modeling difficulties intrinsic to other numerical approaches and that play a significant role in this context of applications, such as the discretization of thin conductors and of large inactive air regions.

The analysis of capacitive coupling situations or the account of capacitive effects are not contemplated in this work and are left for future developments.

We expect this work to help to lay the groundwork for the analysis of complex, large scale three-dimensional electromagnetic coupling situations occurring in the outskirts of overhead lines from the point of view of computational electromagnetics.

1.4 Electromagnetic model

In order to achieve these objectives, the following chapters will discuss the modeling of coupling phenomena and the solution of the numerical problems arising from the proposed electromagnetic models. This section is devoted to stating the basic relations governing the relevant electromagnetic effects for later reference.

The coupling of an overhead transmission line with an arbitrary adjacent system is governed by Maxwell's equations. This is the case of all electromagnetic phenomena in macroscopic media, and the categorization of coupling effects into the three independent classes stated in section 1.2 is conceived only as an aid to the analyst.

Maxwell's equations relate the electromagnetic fields to their ultimate sources, which are the free electric volume charge density ρ_V and the electric current density distribution $\mathbf{J}$. These equations are given below:

$$\nabla \times \mathbf{E} = -\frac{\partial \mathbf{B}}{\partial t}; \tag{1.1a}$$

$$\nabla \times \mathbf{H} = \mathbf{J} + \frac{\partial \mathbf{D}}{\partial t}; \tag{1.1b}$$

$$\nabla \cdot \mathbf{B} = 0; \tag{1.1c}$$

$$\nabla \cdot \mathbf{D} = \rho_V. \tag{1.1d}$$

Each field occurring in the set of equations given by (1.1) is pairwise related to a counterpart by means of the appropriate constitutive relations of the material media. As usual, the relationship between magnetic flux density $\mathbf{B}$ and magnetic intensity $\mathbf{H}$ is written as

$$\mathbf{B} = \mu \mathbf{H}. \tag{1.2}$$

For electric flux density $\mathbf{D}$ and for electric field intensity $\mathbf{E}$,

$$\mathbf{D} = \varepsilon \mathbf{E}. \tag{1.3}$$

Similarly, Ohm's law establishes the relationship between electric field $\mathbf{E}$ and the current density $\mathbf{J}$:

$$\mathbf{J} = \sigma \mathbf{E} = \rho^{-1} \mathbf{E}. \tag{1.4}$$

In the most general case, electric permittivity ε, magnetic permeability μ, electric conductivity σ and electric resistivity $\rho = \sigma^{-1}$ are tensors reflecting the particular behavior of the media. In the applications later considered in this work, only simple scalar material properties will be taken into account.

The continuity equation for electric currents given by

$$\nabla \cdot \mathbf{J} + \frac{\partial \rho_V}{\partial t} = 0 \tag{1.5}$$

is implied by (1.1b). Additionally, the absence of free magnetic poles expressed by (1.1c) is consistent with the following definition of a magnetic vector potential $\mathbf{A}$:

$$\mathbf{B} = \nabla \times \mathbf{A}. \tag{1.6}$$

Seeing that the order of space and time derivatives may be interchanged, Faraday's induction law (1.1a) may be restated with the aid of (1.6) in the form given below:

$$\nabla \times \left(\mathbf{E} + \frac{\partial \mathbf{A}}{\partial t} \right) = 0. \tag{1.7}$$

This leads to the introduction of a scalar electric potential φ as well, since the quantity in the left-hand side of (1.7) with a vanishing curl can be expressed as the gradient of some scalar function:

$$\mathbf{E} + \frac{\partial \mathbf{A}}{\partial t} = -\nabla \varphi \,. \tag{1.8}$$

The foregoing relations will be eventually retaken in the course of the next chapters.

1.5 Organization of this document

This introduction will be followed by five other chapters, and the conceptual separation of coupling phenomena into the categories described in section 1.2 is reflected in their organization.

Chapter 2 begins with a review of the technical literature concerned with electromagnetic coupling phenomena in the context of power systems. Special attention will be dedicated to numerical approaches employed in the analysis of this class of applications.

The next two chapters will be devoted to the finite element analysis of con-

ductive coupling phenomena in the vicinities of an overhead line. In chapter 3, a special boundary condition will be proposed, in order to circumvent the modeling difficulties related to the representation of a soil domain with open boundaries. This approach will be tested in chapter 4 in an assortment of cases of application.

Chapter 5 is dedicated to modeling inductive coupling situations with the generalized PEEC method. The solution of a particular inductive coupling problem will be considered, and the results will be confronted with the alternative solutions obtained with the finite element method.

Finally, chapter 6 will conclude this document with a critical evaluation of the developments. The proposition of possible extensions or future works will be outlined as well.

2 BIBLIOGRAPHIC REVIEW

2.1 Introduction

The modeling of electromagnetic coupling phenomena involving overhead lines in power systems has evolved over the course of time. Different approaches have been employed throughout the years, and in this chapter an account of the research dedicated to its modeling will be presented.

This review is organized in three parts. The first two are mostly concerned with the earliest theoretical developments and with the transition to a later period characterized by the introduction of digital computers in this field of study. These are followed by a section dedicated to the use of specific numerical methods in this domain of applications, with emphasis on the Finite Element Method (FEM) and the Partial Element Equivalent Circuit (PEEC) Method.

2.2 Early developments

While the turn of the nineteenth century to the twentieth is characterized by the consolidation of AC polyphase systems as the preferred power transmission method, the ensuing decades observed a wide dissemination of large-scale, high-voltage power grids all over the world. Not by chance, the investigations concerned with the electromagnetic coupling between power transmission systems and nearby structures may be traced back to that time.

In that period, the diffusion of power transmission networks had already resulted in their significant proximity with other systems, leading to the hazardous effects discussed in section 1.2. In accordance with the resources then available, the modeling attempts were based on purely analytical techniques.

For instance, classical works such as (CARSON, 1926) and (POLLACZEK, 1926; POLLACZEK, 1931) laid the groundwork for the analysis of the inductive coupling between overhead lines and parallel structures in the presence of a conductive soil. Similarly, works such as (OLLENDORFF, 1928) and (STEFANESCO; SCHLUMBERGER; SCHLUMBERGER, 1930) provided the basic tools for investigating the flow of electrical currents in stratified soils and for analyzing conductive coupling phenomena.

By the mid-twentieth century, the number and variety of systems coexisting with power transmission utilities had grown to the point of being a source of concern. The work by (SUNDE, 1949) belongs to this particular period and compiles the methods of analysis available at the time in this domain of applications. Meanwhile, a better quantitative understanding of the risks of electric shock was also attained (DALZIEL, 1956), reinforcing the care with working personnel in shared rights of way.

The growing concern with electromagnetic coupling problems is manifested in the continuous discussion of related topics in the specialized literature (POHL, 1966; FAVEZ; GOUGEUIL, 1966; DAWALIBI; MUKHEDKAR, 1975). The modeling of grounding electrodes and the study of coupling situations between overhead lines and underground parallel pipelines are among the applications most frequently considered. The continued and cumulative discussions on these themes led different institutions to organize special research commissions, which eventually produced an extensive technical documentation composed of reports (FRAZIER, 1984; DAWALIBI et al., 1988), engineering

guides (CIGRÉ, 1995) and standards (CENELEC, 2012).

The second half of the twentieth century is marked by the advent of the digital computer as well, which influenced the modeling of this class of problems. The resulting trends in the development of numerical techniques for analyzing electromagnetic coupling with overhead lines will be covered in the following section.

2.3 Trends in computer modeling

A first modeling trend that benefited from the increasing availability of computer resources is expressed by the development of special purpose software tools based on semi-analytical procedures. The approaches belonging to this group may be regarded as computer implementations of the well-established analytical techniques previously mentioned, which were frequently too laborious to be of practical use without the aid of a computer.

The software solutions issued from this trend are particularly well suited to the analysis of the inductive coupling between overhead lines and long parallel structures, since they rely on the analytical evaluation of self and mutual inductances. The computations are frequently organized in zones of approximate parallelism and lead to the assembly of a large equivalent network of lumped circuit elements (DAWALIBI, 1980; SOBRAL et al., 1991). The works by (DAWALIBI; SOUTHEY, 1989) stand out in this category, since their contemporary software implementations have become popular in specialized power engineering communities and have found a commercial success (SES, 2015).

The second recognizable trend corresponds to the use of general numerical techniques to analyze electromagnetic problems. Early examples of efforts in the discipline of computational electromagnetics include the works by (YEE,

1966) with the Finite Difference Method and by (SILVESTER, 1969; SILVESTER; CHARI, 1970) with the Finite Element Method. The Partial Element Equivalent Circuit technique may be traced back to the work by (RUEHLI, 1974).

These pioneering works in the domain of computational electromagnetics were concerned with specific problems, such as wave propagation, non-linear magnetostatics and equivalent circuit determination. In spite of this, a diversification in the use of the corresponding general numerical techniques was eventually attained, reaching the analysis of electromagnetic coupling problems involving overhead lines in power systems. Some relevant applications will be discussed in the following section.

2.4 Numerical analysis of conductive and inductive coupling applications

The modeling of conductive coupling problems is closely related to the analysis of grounding systems. Various numerical techniques have been employed to model this class of problems, ranging from integral approaches to the use of the Finite Element Method.

The first works based on the FEM for analyzing grounding systems were based on static nodal formulations (CARDOSO, 1994; TRLEP; HAMLER; HRIBERNIK, 1998). Time harmonic formulations still based on nodal elements were introduced by (NEKHOUL et al., 1995; NEKHOUL et al., 1996), and the use of edge elements was introduced by (SILVA, 2006; SILVA et al., 2007). A comprehensive account on the development of FEM formulations for the analysis of grounding systems is provided in (SILVA, 2006).

The modeling of this class of applications with the FEM has been preferred by some analysts due to some of its intrinsic characteristics. Among the most

significant ones is that FEM-based approaches lead to the solution of sparse systems of equations, which are much more easily treatable from a numerical point of view. The account of non-homogeneous and non-linear media with this method tends to be simplified as well, when compared to integral approaches.

On the other hand, the standard FEM is not well adapted to the treatment of open boundaries, which occur in the representation of underground regions. As a consequence, several efforts have been undertaken to circumvent these limitations. Simple domain truncation, infinite elements (ZIENKIEWICZ; TAYLOR; ZHU, 2006; DHATT; TOUZOT; LEFRANÇOIS, 2007), coordinate transformations (STOHCHNIOL, 1992; CARDOSO, 1994) and the use of fictitious absorbers (perfectly matched layers, or PML) on the outer boundaries of the representation (BERENGER, 1994; SILVA, 2006) are among the techniques employed together with the FEM in this context. The inadequacy of these techniques to the finite element analysis of complex conductive coupling situations will be discussed in chapter 3, together with the proposal of an alternative scheme adapted to this extended context of applications.

The finite element analysis of inductive coupling phenomena has been proposed as well. The specific problems of application considered tend to be limited to situations involving the parallelism of long structures with overhead lines in a common right of way, in order to profit from 2-D FEM formulations. Examples can be found in the works by (SATSIOS; LABRIDIS; DOKOPOULOS, 1998) and (CHRISTOFORIDIS; LABRIDIS; DOKOPOULOS, 2005).

General 3-D inductive coupling problems involving overhead lines are characterized by large inactive volumes of air separating the phase wires (i.e. the inductor) and the regions or devices subjected to induction. Since the FEM cannot avoid the discretization of these inactive air regions, mesh generation complications, large memory requirements and long computation times are to

be expected in this case. On the other hand, integral approaches such as the PEEC method are capable of modeling this kind of interaction without discretizing the air.

The classical PEEC method is particularly well-adapted to modeling devices composed of interconnected parts, in which the current density is characterized by a well-defined direction and by an approximately uniform intensity. This is particularly the case of printed circuit board tracks, integrated circuits interconnections and power electronic devices. Applications belonging to the domain of power systems engineering are rare. Works modeling the transient response of high-voltage towers and grounding systems to lightning strikes by (ANTONINI; CRISTINA; ORLANDI, 1997) and by (YUTTHAGOWITH et al., 2011) are among the few examples of applications of the PEEC method to this area.

More recently, generalized versions of the basic PEEC technique were proposed using alternative approximations for the current density (NGUYEN et al., 2014), allowing the treatment of eddy current problems in massive conductors and the penetration of the method into other niches of application. An extensive account of the development and of the use of the PEEC method and other related techniques is provided by (NGUYEN, 2014).

2.5 Chapter summary

This chapter presented a brief and non-exhaustive account of the works available in the technical literature concerned with modeling electromagnetic coupling effects in power systems.

In the case of the finite element analysis of conductive coupling phenomena, most of the applications can be said to be concerned with the analysis of independent grounding systems, for which traditional domain truncation tech-

niques are applicable. In the case of inductive coupling problems, the most frequently analyzed situations involve the parallelism of elongated structures with the overhead line along great distances.

The developments discussed from now on in the following chapters are expected to contribute to the numerical modeling of the electromagnetic phenomena involved, as well as to better understanding such coupling interactions.

3 CONDUCTIVE COUPLING MODELING

3.1 Introduction

This chapter analyzes the numerical modeling of conductive coupling problems in transmission line rights of way. As already discussed, this category of problems derives from the injection of electrical currents in the soil, leading to the establishment of an electromagnetic field beneath the earth surface. Living subjects roaming the vicinities of the region where the current injection takes place may be exposed to dangerous effects; underground structures and devices may be damaged.

The modeling of such a class of applications is closely related to the analysis of grounding systems, since the electric currents diverted from an overhead line are injected into the earth by means of earthing electrodes. As a consequence, finite element method techniques already employed for modeling that former class of applications may be extended and adapted in the analysis of the latter.

The following sections will describe the problem in detail and will highlight the complications involved in modeling conductive coupling phenomena in comparison with the finite element analysis of a simple grounding system. As will become clear, these difficulties are mostly concerned with the truncation of the computational domain and with the application of a representative

boundary condition to its frontiers.

3.2 Distribution of fault currents diverted to the ground during a contingency

Overhead transmission lines provide the interconnection between electric power generation sites and electric power consumers. The length of the transmission system is often considerable, and a great number of towers may be required to span the distances involved. Along the path followed by the line, each tower is anchored to the ground by its foundation and is electrically connected to the earth by means of a grounding network.

While the energized conductors integrating the power transmission circuit are supported by the towers and attached to them by means of insulators, a complementary circuit composed of shield or guard wires is held at a higher level and in direct contact with their metallic structures. These shield wires are expected to protect the energized conductors from direct lightning strikes.

This particular configuration in which the tower structures are interconnected by the shield wires makes an effective path for electric currents to flow towards the earth during a contingency. In case of a lightning strike or during the failure of an insulator in one of the towers, a complicated and non-trivial pattern of electric currents is injected into the ground at the tower footings.

Figure 4 depicts a schematic representation of the situation just portrayed and highlights the fact that the fault current may spread to distances far away from the fault point. Each of the current components I_k flowing into the earth may be regarded as a possible cause of conductive coupling phenomena in the vicinities of the overhead line. Their intensities may be either determined by a system-wide computation (DAWALIBI; BENSTED; MUKHEDKAR, 1981) or mea-

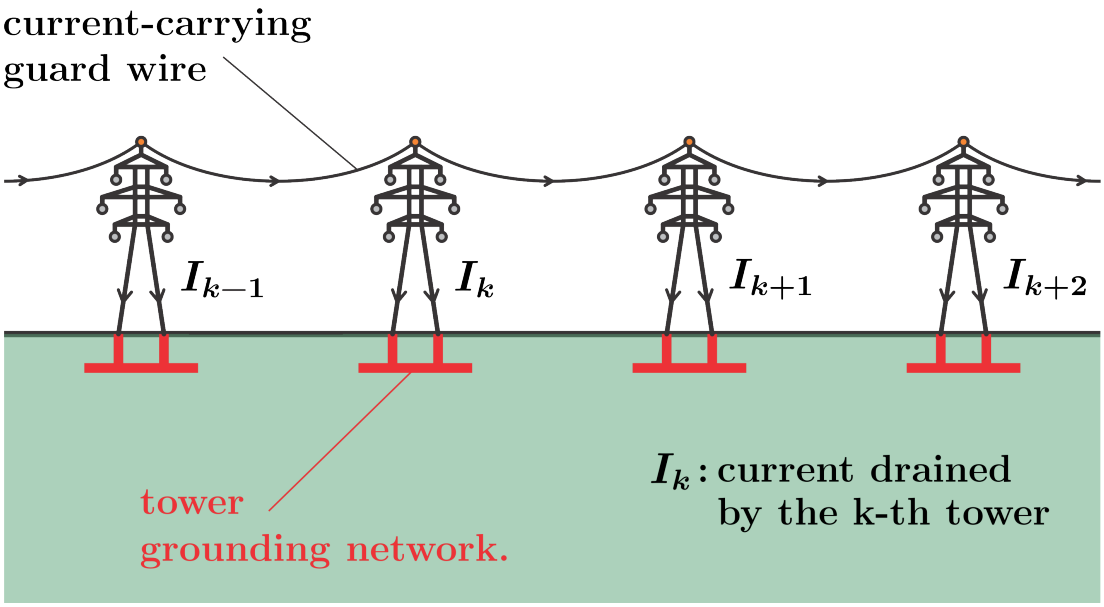

Figure 4: Ground current distribution in a faulted overhead line.

sured directly by an appropriate experimental arrangement (SEBŐ; RÉGENI, 1963).

Even though this pattern $\{I_k\}$ of injected currents can be predicted or determined, its distribution along the large region traversed by the overhead line makes it difficult to ascertain a priori the effective extent of the area subjected to their influences. This represents a major difficulty for modeling this class of electromagnetic phenomena with numerical methods, as will be discussed in the next section.

3.3 Modeling the flow of electric currents in the context of conductive coupling phenomena

The flow of electric currents in a three-dimensional domain can be investigated with the aid of analytical and numerical techniques. In this section, the modeling of this class of problems will be first described in general terms. The adaptions to the analysis of conductive coupling phenomena in the vicinities of a power system will be discussed thereafter.

3.3.1 Formulation of the boundary value problem

Conductive coupling phenomena in transmission line rights of way can be conveniently modeled as steady state electric conduction problems. Under these circumstances, the time derivatives occurring in Maxwell's equations (1.1) are neglected. As a consequence, the continuity equation expressed by (1.5) becomes simply

$$\nabla \cdot \mathbf{J} = 0. \tag{3.1}$$

The relationship between electric field $\mathbf{E}$ and scalar potential φ provided by (1.8) is also reduced to

$$\mathbf{E} = -\nabla\varphi. \tag{3.2}$$

With the aid of (1.4) and (3.2), (3.1) can be recast in terms of φ, leading to the following boundary value problem in a conductive domain Ω:

$$\nabla \cdot (-\sigma \nabla\varphi) = 0 \text{ in } \Omega; \tag{3.3a}$$

$$\varphi = \varphi_0 \text{ in } \Gamma_D; \tag{3.3b}$$

$$-\sigma \nabla\varphi \cdot \mathbf{n} = | \mathbf{J}_0 | \text{ in } \Gamma_N. \tag{3.3c}$$

Equation (3.3a) requires boundary conditions to ensure the uniqueness of its solution. These conditions are expressed by constraints (3.3b) and (3.3c), which are defined upon two complementary surfaces denoted by Γ_D and Γ_N. These surfaces together enclose the domain completely, and the unit vector pointing outward from Ω on these boundaries is designated by $\mathbf{n}$.

These facts are represented schematically in Figure 5. The constraint expressed by (3.3b) is a Dirichlet boundary condition enforcing a prescribed potential φ_0 upon Γ_D, whereas (3.3c) is a Neumann boundary condition imposing

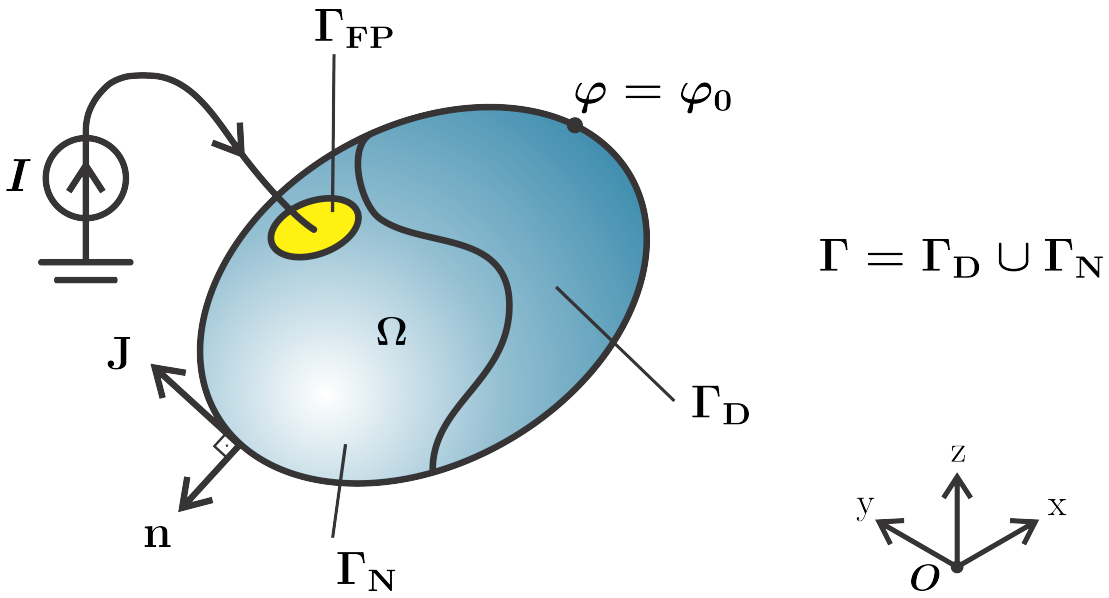

Figure 5: Bounded conductive domain illustrating a steady state current conduction problem, excited by a current source.

a specified normal current density entering Ω through Γ_N. This condition is assumed to be homogeneous (i.e. $|\mathbf{J}_0| = 0$) everywhere on Γ_N, with the exception of Γ_{FP} where current injection takes place (with index FP standing for “fault points”).

This general definition of a boundary value problem may be employed to investigate a wide range of applications that include conductive coupling phenomena involving overhead lines in their rights of way. Figure 6 provides a graphical representation of the associations that will be established in the following paragraphs between the abstract general problem depicted in Figure 5 and the situation shown in Figure 4.

Indeed, under the circumstances exposed in section 3.2, Ω may be associated to an underground region of soil into which electric currents are fed by means of grounding electrodes. The cross sections of these electrodes at the ground surface are then identified with Γ_{FP} and with the non-homogeneous boundary condition (3.3c).

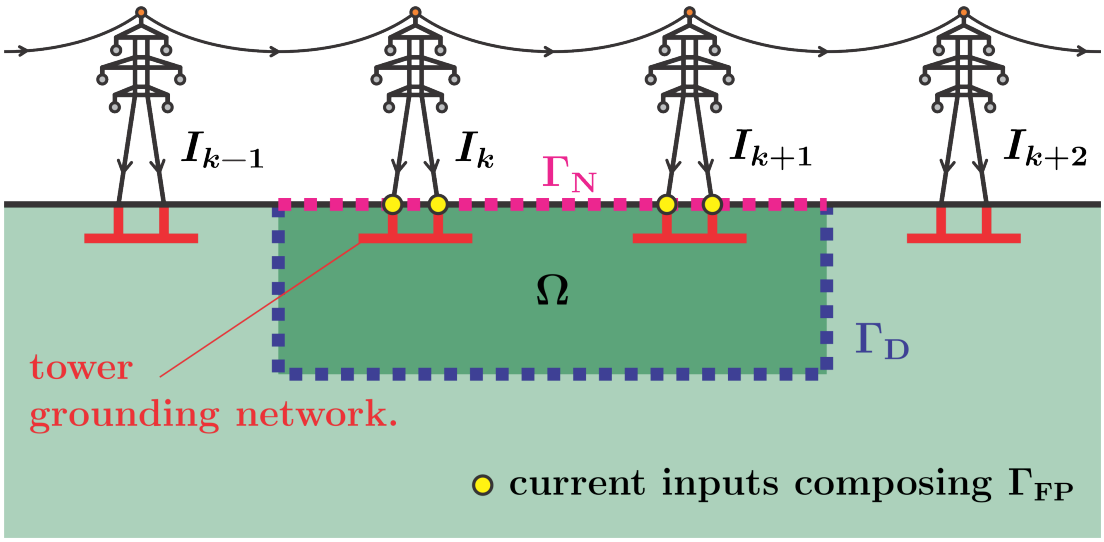

Figure 6: Sketch of a transmission line right of way profile, showing the truncated region (dark green) chosen as the conductive domain for modeling steady state conduction phenomena.

The air-soil interface is a Γ_N-type surface due to the continuity conditions on the normal component of $\mathbf{J}$. Moreover, displacement currents are nonexistent in the steady state, allowing the identification of this boundary with the Neumann condition (3.3c) in its homogeneous version ($|\,\mathbf{J}_0\,| = 0$).

The remaining boundary surface required to fully enclose Ω is completely beneath the soil surface. It may be promptly identified with Γ_D and its corresponding Dirichlet condition (3.3b). The choice of an appropriate electric potential distribution φ_0 on Γ_D in this case is critical for obtaining a consistent solution for the current flow inside Ω, and this subject will be the focus of the following sections of this chapter.

3.3.2 Imposing a vanishing potential condition at infinity

The physical condition most frequently imposed on the analysis of problems involving the underground flow of electrical currents is that φ vanishes at distances sufficiently far away from the current electrodes. Indeed, this condition is either implicitly or explicitly enforced in the analytical solution of simple

grounding configurations.

In the framework of the boundary value problem established in the previous section, the enforcement of this condition corresponds to the assumptions that boundary Γ_D is located at infinity and that the Dirichlet constraint in (3.3b) becomes homogeneous with $\varphi_0 = 0$. As a consequence, domain Ω is reduced to a half-space bounded only by the air-soil interface.

When numerical techniques are considered for dealing with complex but secluded grounding systems, this condition of a vanishing electrical potential may still be emulated. For instance, the finite element method relies upon the discretization of a geometrical model of the region under analysis that must be inevitably limited and finite. As a consequence, it cannot deal directly with a boundary taken to infinity, but suitable techniques can enforce or at least approximate the required physical condition for the potential.

Among the techniques available for circumventing this limitation, the simplest one corresponds to the mere over-dimensioning of the computational domain, which leads to an approximate solution. As seen on chapter 2, more sophisticated methods include the use of spatial transformations (CARDOSO, 1994), infinite elements (ZIENKIEWICZ; TAYLOR; ZHU, 2006; DHATT; TOUZOT; LEFRANÇOIS, 2007) and of perfectly matched layers (BÁRDI; BÍRÓ; PREIS, 1998).

However, the foregoing procedures are only formally acceptable when applied to the analysis of simple and secluded grounding systems. None of them are strictly suitable for dealing with a transmission line right of way. The reason behind these assertions is that any of these approaches would implicitly neglect the contributions added by the current injections in every tower footing left outside the geometrical model, as represented schematically in Figure 7.

To judge a priori whether or not the neglect of these current injections tak-

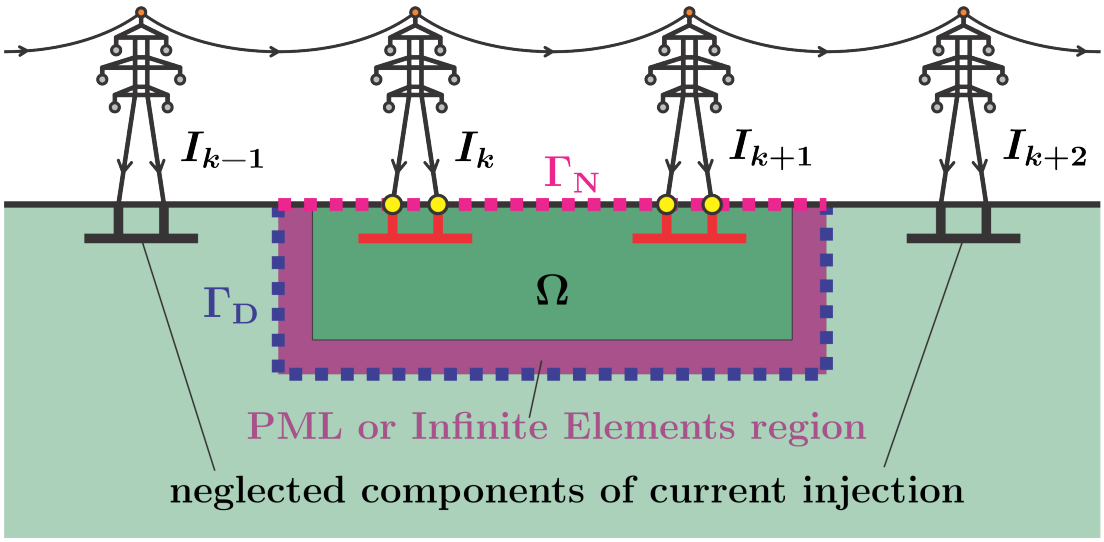

Figure 7: Conductive domain delimited by the dotted line. The purple region is the one where truncation techniques are to be applied (either PML or infinite element).

ing place beyond the truncation boundaries would provide an acceptable approximation in the finite element analysis of a particular conductive coupling problems is a difficult task. In order to avoid this dilemma, a procedure that tries to take these current contributions into account is proposed in this chapter.

The technique proposed consists in computing a non-homogeneous Dirichlet boundary condition for every point lying on boundary Γ_D by means of a conveniently defined function. The explicit form of this function will arise from the investigation carried out in the following section.

3.4 Analytical solution and asymptotic behavior of selected grounding arrangements

In the following subsections, the analytical solution of some selected problems will be considered. The intended objective is to make explicit the asymptotic behavior of the solutions obtained for φ at far away distances in different

situations. The results will motivate the definition of a particular function φ_0 defined on Γ_D, in order to determine a more convenient version of the boundary condition (3.3b) to analyze conductive coupling problems occurring in the vicinities of a faulted transmission system.

Three particular configurations will be addressed:

- A point current source injecting current into the ground;
- A very long horizontal electrode buried deep under the soil surface and
- A finite vertical grounding rod driven into the soil.

3.4.1 The electric potential of a point current source

Firstly, let the problem of a point current source lying on the earth surface be considered as shown in Figure 8. As discussed in the previous section, in this case domain Ω corresponds to a semi-space bounded only by the interface between the earth and the air, and Γ_D is supposed to be far away from the point source at infinity.

The point source is supposed to be located at the origin of a system of coordinates and injects a total current I into Ω. This domain is supposed to be composed by a homogeneous and isotropic soil of conductivity σ_S. In this idealized situation, the total electric current I fed by the source into the medium spreads towards infinity with a uniform distribution. Consequently, the geometric loci of constant current densities $|\mathbf{J}|$ are semi-spherical shells concentric to the point source.

Any point located on one of these shells may be represented by a position vector $\mathbf{r}$. The current density evaluated at such a point will be accordingly

$$\mathbf{J}(\mathbf{r}) = \frac{I}{2\pi |\mathbf{r}|^2} \frac{\mathbf{r}}{|\mathbf{r}|}. \tag{3.4}$$

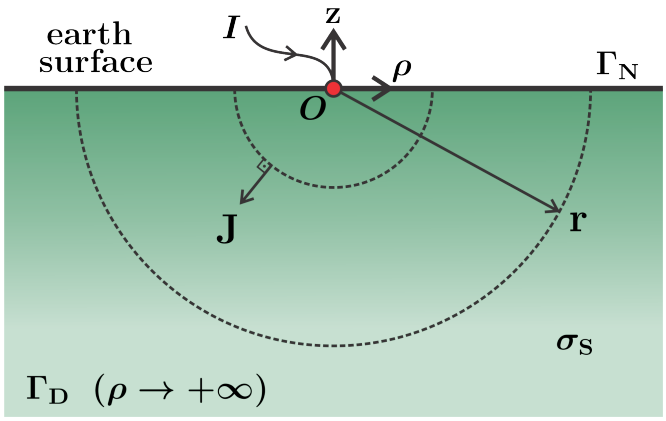

Figure 8: A point current source lying on the soil surface.

The electric field $\mathbf{E}$ distribution associated to this current flow is related to (3.4) by means of Ohm's law (1.4). Since the electric potential at infinity is assumed to be $\varphi_0 = 0$, the integration of $\mathbf{E}$ along a convenient radial path yields the electric potential at $\mathbf{r}$:

$$\varphi(\mathbf{r}) = -\int_{\infty}^{\mathbf{r}} \mathbf{E}(\mathbf{R}) \cdot d\mathbf{R} = -\frac{I}{2\pi\,\sigma_S} \int_{\infty}^{\mathbf{r}} \frac{\mathbf{R}}{|\mathbf{R}|^3} \cdot d\mathbf{R} = \frac{I}{2\pi\,\sigma_S\,|\mathbf{r}|}. \tag{3.5}$$

This expression may be rewritten with the expansion of $|\mathbf{r}|$ into variables ρ and z of a cylindrical system of coordinates centered at the point charge, as shown below:

$$\varphi = \frac{I}{2\pi\,\sigma_S\,|\mathbf{r}|} = \frac{I}{2\pi\,\sigma_S\,\sqrt{\rho^2 + z^2}}. \tag{3.6}$$

Any of these expressions may be easily shown to satisfy the partial differential equation corresponding to (3.3a) by means of differentiation and direct substitution.

As already emphasized, the previous expressions were obtained for a point current source injecting a current I into a semi-infinite half-space Ω. If the related problem of a point current source inside a homogeneous and isotropic medium unbounded in all directions was considered, an analogous expression for the resulting electric scalar potential could be obtained by similar proce-

dures. The result would be simply

$$\varphi = \frac{I}{4\pi\,\sigma_S\,|\mathbf{r}|} = \frac{I}{4\pi\,\sigma_S\,\sqrt{\rho^2+z^2}}, \tag{3.7}$$

which is half of the potential predicted by (3.6).

Both (3.6) and (3.7) show that the potential of a point source varies inversely with the radial distance measured from the source.

3.4.2 The electric potential of a horizontally buried cylindrical electrode

A second analytical problem will be considered in this section, which corresponds to an idealization of a sufficiently long ground wire buried horizontally and deep into the earth. It corresponds to a cylindrical conductor of infinite length and radius R embedded in an unbounded soil domain Ω, as shown in Figure 9.

The conductivities of the soil and of the conductor will be denoted by σ_S and σ_C respectively. A cylindrical system of coordinates attached to the conductor is also shown in Figure 9 and a direct electrical current I is injected in its origin. This current travels through the conductor and is drained into the soil, leading to an electric potential distribution φ that satisfies (3.3a).

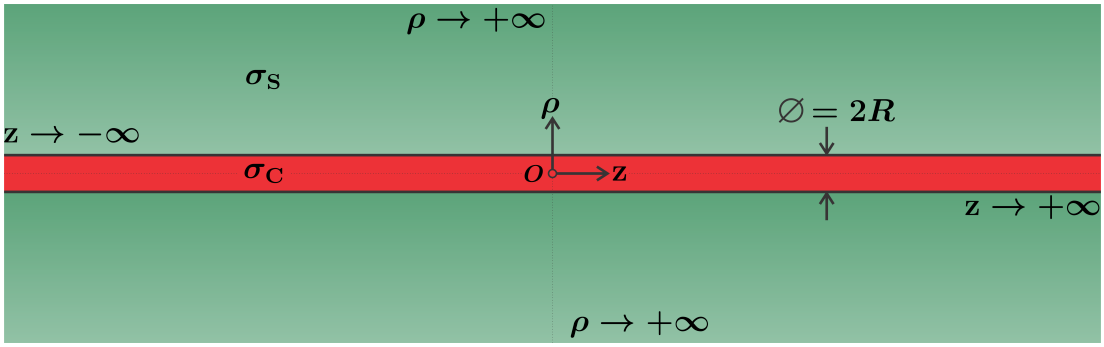

Figure 9: The long cylindrical conductor embedded in an infinite medium analyzed by (OLLENDORFF, 1926).

It is convenient in this case to express electric potential φ in terms of a piecewise-defined function, for which the region inside the conductor is distinguished from the soil. More specifically,

$$\varphi(\rho,z)=\begin{cases}\varphi_C(\rho,z) \text{ if } \rho \le R,\\ \varphi_S(\rho,z) \text{ if } \rho \ge R.\end{cases} \tag{3.8}$$

The functions defined in the two sub-regions are related to each other at the interface between the conductor and the soil $(\rho = R)$ by means of the appropriate continuity conditions. Electric potential φ and the normal component of current density vector $\mathbf{J}$ must be single-valued in the interface. Taking (1.5) into account, these conditions become

$$\varphi_C(R,z)=\varphi_S(R,z), \tag{3.9a}$$

$$\sigma_{\mathrm{C}}\left.\frac{\partial\varphi_c}{\partial\rho}\right|_{(\rho=R)}=\sigma_{\mathrm{S}}\left.\frac{\partial\varphi_S}{\partial\rho}\right|_{(\rho=R)}. \tag{3.9b}$$

Additionally, these functions are expected to vanish at infinity as follows:

$$\lim_{z\to\infty}\varphi_C(\rho,z)=0 \text{ for } \rho \le R, \tag{3.10a}$$

$$\lim_{z\to\infty}\varphi_S(\rho,z)=0 \text{ for } \rho \ge R. \tag{3.10b}$$

The boundary value problem previously described was investigated in detail by (OLLENDORFF, 1926; OLLENDORFF, 1928). The analytical solutions obtained are expressed by means of integrals involving Bessel and Hankel functions, as expected in the case of Laplace problems involving symmetries about an axis. In particular, the electric potential in the soil region was shown to be:

$$\varphi_S(\rho,z)=\frac{I}{4\pi\sigma_{\mathrm{S}}R}\int_0^\infty\frac{2}{\pi\Lambda}\frac{jH_0^{(1)}\left(j\Lambda\frac{\rho}{R}\right)\cos\left(\Lambda\frac{z}{R}\right)}{J_0(j\Lambda)H_0^{(1)}(j\Lambda)-\frac{\sigma_{\mathrm{C}}}{\sigma_{\mathrm{S}}}J_1(j\Lambda)H_1^{(1)}(j\Lambda)}\,\mathrm{d}\Lambda. \tag{3.11}$$

The asymptotic behavior of this equation for positions far away from the

conductor (i.e., $\rho/R \to \infty$) may be obtained by taking the denominator of the previous expression to the limit $\Lambda \to 0$ (OLLENDORFF, 1926). This limiting procedure leads to

$$\lim_{\rho\to\infty} \varphi_S\,(\rho, z) = \frac{I}{4\pi\sigma_S R} \int_0^\infty jH_0^{(1)}\left(j\Lambda\frac{\rho}{R}\right)\cos\left(\Lambda\frac{z}{R}\right)\mathrm{d}\Lambda. \tag{3.12}$$

The integral representation provided by the previous equation can be restated in terms of simple analytic functions. More specifically, it may be demonstrated (BOLLIGER, 1917) that

$$\frac{I}{4\pi\sigma_S R} \int_0^\infty jH_0^{(1)}\left(j\Lambda\frac{\rho}{R}\right)\cos\left(\Lambda\frac{z}{R}\right)\mathrm{d}\Lambda = \frac{I}{4\pi\ \sigma_S\ \sqrt{\rho^2+z^2}}. \tag{3.13}$$

The comparison of (3.13), (3.12) and (3.7) lead to the conclusion that the asymptotic behavior of the electric potential produced by the cylindrical conductor at far away distances is equivalent to the one of a point current source.

3.4.3 The electric potential of a vertically buried rod

The last problem analyzed in this series is shown schematically in Figure 10(a). It corresponds to a thin cylindrical conductor that is vertically driven into the soil. This electrode drains a total current I and its length ℓ is much longer than its radius R. This soil conductivity is once again represented by σ_S.

Among the different approaches for analyzing the behavior of the electric potential arising in this case, the one provided by (RÜDENBERG, 1945) is particularly convenient to investigate its asymptotic behavior at distances far away from the electrode. The procedure proposed in that work is partially adapted in what follows to achieve this objective.

Instead of formally solving the boundary value problem in this case, the procedure bases itself on the assumption that the current leaving the electrode

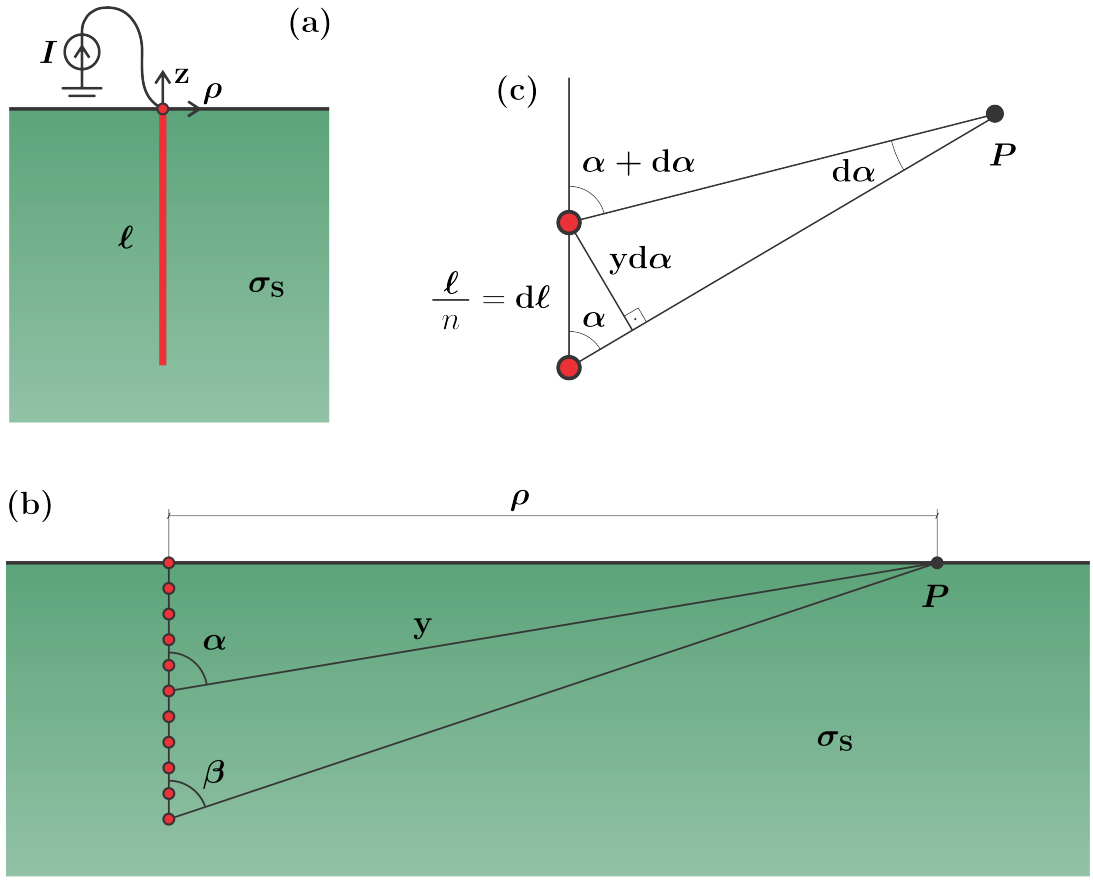

Figure 10: The grounding rod analyzed by (RÜDENBERG, 1945) (a), its substitution by point current sources (b) and some geometrical relations valid for distant P (c).

and entering the soil is uniformly distributed along its length, and that the contributions of an element of length of the rod to the total electric potential may be added based on the principle of superposition of effects.

More specifically, the vertical electrode is replaced by a large number n of point current sources evenly disposed along length ℓ, each one injecting a current I/n into the soil as depicted in Figure 10(b). Each point source is accompanied by its corresponding image source placed symmetrically about the earth surface in order to take into account the finiteness of the soil domain.

Let then y be the distance between one of these point sources and a point P lying on the soil surface. According to (3.7), the electric potential created by each of these sources and at this point will then be

$$\mathrm{d}\varphi = \frac{2\left(I/n\right)}{4\pi\,\sigma_S\,y}, \tag{3.14}$$

in which the extra multiplying factor 2 takes into account the contribution provided by the image source.

This distance y may be rewritten in terms of geometric parameter α, which corresponds to the angle shown in Figure 10(b). According to the diagram of Figure 10(c), for large n and for a point P far away from the rod, the following relations hold true:

$$\mathrm{d}\ell = \frac{\ell}{n}\;; \quad \sin\alpha = \frac{y\,\mathrm{d}\alpha}{\mathrm{d}\ell}\;; \quad y = \frac{\ell\,\sin\alpha}{n\,\mathrm{d}\alpha}. \tag{3.15}$$

As a consequence, the potential contribution provided by each point source may be restated as

$$\mathrm{d}\varphi = \frac{2\left(I/n\right)}{4\pi\,\sigma_S\,\dfrac{\ell\,\sin\alpha}{n\,\mathrm{d}\alpha}} = \frac{I}{2\pi\,\sigma_S\,\ell}\frac{\mathrm{d}\alpha}{\sin\alpha}. \tag{3.16}$$

The total potential resulting at point P can then be obtained by integration along the rod, with limits going from $\alpha = \beta$ (the limiting angle shown in the diagram, corresponding to the tip of the rod) to $\alpha = \pi/2$:

$$\varphi = \frac{I}{2\pi\,\sigma_S\,\ell}\int_{\beta}^{\pi/2}\frac{1}{\sin\alpha}\,\mathrm{d}\alpha = \frac{I}{2\pi\,\sigma_S\,\ell}\,\ln\left(\frac{1+\cos\beta}{\sin\beta}\right). \tag{3.17}$$

Furthermore, L'Hôpital's rule may be employed to show that

$$\lim_{\beta\to\pi/2}\frac{\ln\left(\dfrac{1+\cos\beta}{\sin\beta}\right)}{\cos\beta} = 1. \tag{3.18}$$

As a consequence, and since $\beta \to {}^{\pi}/_{2}$ corresponds to the evaluation of the potential at a point far away from the rod,

$$\varphi = \frac{I}{2\pi\,\sigma_S\,\ell}\,\cos\beta. \tag{3.19}$$

However, at large distances $\cos\beta = {}^{\ell}/_{y} \approx {}^{\ell}/_{\rho}$. This substitution into (3.19) finally leads to

$$\varphi = \frac{I}{2\pi\,\sigma_S\,\rho}, \tag{3.20}$$

which is once again identifiable with the potential created by a point source (3.6).

3.5 Domain truncation by non-homogeneous Dirichlet boundary condition

The results compiled in the previous section show that different problems involving the dispersion of currents in the soil resulted in the same asymptotic behavior for the electric potential, when positions far away from the point of current injection are considered. In this sense, both grounding configurations examined in sections 3.4.2 and 3.4.3 could be replaced by an equivalent point current source injecting the same current into the soil if only outlying regions were considered for evaluating the electric potential.

Additionally, the procedure employed in the analysis of section 3.4.3 introduces the possibility of superposing the effects of point current sources in this context of applications in order to compose or to build the solution of a more complex problem.

These observations regarding the superposition of point current sources suggest that similar concepts may be adopted to address the difficulties highlighted in section 3.3.2. If the foregoing notions are generalized, an alternate

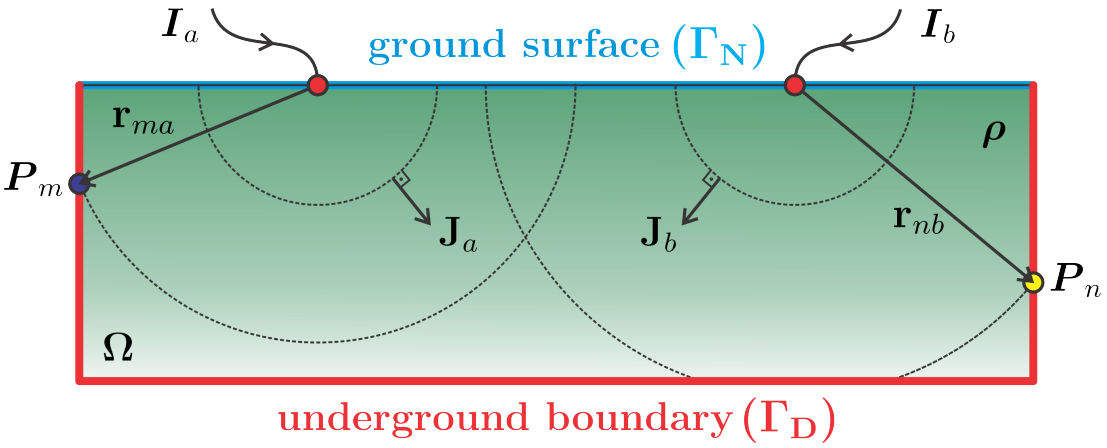

Figure 11: Schematic representation of domain Ω for computing the proposed non-homogeneous Dirichlet boundary condition on Γ_D.

scheme for determining the Dirichlet boundary condition (3.3b) upon Γ_D can be envisioned. The approach consists in replacing every tower or structure injecting current in the ground by a point current source lying on the surface of the earth. Each of these sources produces a potential distribution of the form prescribed by (3.6). In the case of N such sources, the superposition of their effects yields the following function φ_0 defined upon Γ_D:

$$\varphi_0\left(P_j\right) = \frac{1}{2\pi\,\sigma_S}\sum_{k=1}^{N}\frac{I_k}{\left|\mathbf{r}_{jk}\right|}. \tag{3.21}$$

Equation (3.21) computes the non-homogeneous Dirichlet boundary condition φ_0 for a generic point P_j lying on Γ_D, as P_m and P_n shown in Figure 11. Distances $\left|\mathbf{r}_{jk}\right|$ are evaluated between the k-th point source on the earth surface and point P_j on Γ_D. As previously discussed in this chapter, quantities I_k are the fault currents shown in Figure 4, which are supposed to be known in advance.

3.6 Solution of conductive coupling problems with the finite element method

Complex conductive coupling problems require numerical solutions of their associated boundary value problem. This section will then discuss the application of the special Dirichlet boundary condition furnished by (3.21) in the context of the finite element method.

Two particular finite element method formulations will be considered. These formulations will be only briefly outlined in the following subsections, since they are well-known numerical procedures. They are namely the classical electrokinetic formulation for solving the problem given by (3.3) and the $\mathbf{A} - \varphi$ formulation. Both of them have been broadly documented in the specialized literature of computational electromagnetics.

Consequently, the reader interested in their full developments is referred to references such as (ZIENKIEWICZ; TAYLOR; ZHU, 2006) and (BÍRÓ, 1999). The reader is also referred to the work by (SILVA, 2006), in which specializations of these formulations dedicated to the analysis of secluded grounding systems and to the computation of their equivalent impedances are presented and thoroughly discussed. The incorporation of the specialized boundary condition proposed in this chapter to the framework of this last reference may be regarded as an extension to the treatment of non-secluded grounding arrangements or, equivalently, to the analysis of conductive coupling problems involving a nearby power system.

Details concerning the modeling of the thin conductors in grounding networks and the current excitation of the finite element model will be covered in this section as well, for the sake of completeness.

3.6.1 Incorporation of the specialized non-homogeneous Dirichlet boundary condition

The use of (3.21) is convenient for solving (3.3) by the finite element method. In this general context, a discretization of Ω in finite elements is required, and in the case of the electrokinetic formulation the following nodal approximation for φ is adopted:

$$\varphi^e = \sum_{i=1}^{nn} \varphi_i^e \, N_i^e . \tag{3.22}$$

Coefficients φ_i^e are the nodal values of φ, and N_i^e are the nodal shape functions. The application of the Galerkin procedure to (3.3) with this approximation ultimately leads to the assembly of a system of equations that has degrees of freedom φ_i^e as its unknowns.

In this scenario, the application of (3.21) consists in identifying points P_j with the mesh nodes lying on boundary Γ_D in order to compute their potentials. The determination of their values allows eliminating the corresponding degrees of freedom φ_i from the assembled system of equations and its subsequent solution.

3.6.2 Generalization to other finite element formulations

The generalization of this boundary value procedure to other formulations of the finite element method developed in terms of a scalar potential may be proposed as well.

Indeed, even though the discussions carried out in this chapter were based on the steady state hypothesis that led to a Laplace type problem, the flow of electric currents in the soil could also have been described by a full wave model. One of the possible approaches admits the sinusoidal variation of the

electromagnetic fields with a frequency ω and employs the magnetic vector potential $\mathbf{A}$ in conjunction with electric scalar potential φ to establish the following differential equation in Ω:

$$\nabla\times(\nu\,\nabla\times\mathbf{A}) + \dot{\sigma}\,(j\omega\mathbf{A} + \nabla\varphi) = 0. \tag{3.23}$$

The potentials in (3.23) are regarded as complex quantities. They are related to each other and to the complex electromagnetic fields $\mathbf{E}$ and $\mathbf{B}$ by (1.6) and (1.8). The material properties ν and $\dot{\sigma} = \sigma + j\omega\varepsilon$ are respectively the reluctivity and the complex conductivity of the media in Ω.

As in section 3.6.1, the finite element analysis of a boundary value problem governed by (3.23) also requires the approximations of $\mathbf{A}$ and φ inside the elements of the mesh. For the case of the vector potential, this approximation may be written as

$$\mathbf{A}^e = \sum_{i=1}^{ne} a_i^e\,\boldsymbol{\omega}_i^e, \tag{3.24}$$

with $\boldsymbol{\omega}_i^e$ belonging to the space of vector edge shape functions and with scalars a_i^e representing degrees of freedom corresponding to the edges of the element. The scalar electric potential, in turn, can be approximated as before by (3.22).

The application of the Galerkin residual procedure to (3.23) with the discretizations expressed by (3.22) and (3.24) leads to a formulation of the $\mathbf{A} - \varphi$ type. As a consequence, the assembled system of equations resulting from the application of the finite element technique to (3.23) will contain both edge degrees of freedom a_i and nodal degrees of freedom φ_i as unknowns.

The presence of the latter category of degrees of freedom allows applying the very same boundary condition scheme previously described for eliminating unknowns φ_i lying on boundary Γ_D. The point source approximation is supposed to remain valid for the substituted grounding electrode in frequency ω.

Besides this assumption, currents I_k of (3.21) are supposed to correspond to their complex phasor representations.

As for the magnetic vector potential $\mathbf{A}$, its tangential component is constrained as follows:

$$\mathbf{n} \times \mathbf{A} = 0 \text{ in } \Gamma = \Gamma_{\mathrm{D}} \cup \Gamma_{\mathrm{N}}. \tag{3.25}$$

This is equivalent to imposing a null outgoing magnetic flux density on the boundary (SILVA, 2006; SILVA et al., 2007) and corresponds to an homogeneous Dirichlet boundary condition on the edge degrees of freedom a_i^e.

3.6.3 Modeling of thin wires

According to the discussion of the preceding sections, the proposed substitution of the current-injecting structures with point current sources allows computing a non-homogeneous Dirichlet boundary condition. It should be remarked, however, that no point source substitution is proposed to the actual representation of the grounding electrodes or of any other structure injecting a component of current into the soil, since such an approach would evidently modify the field solution in Ω at short and intermediate distances from the conductors.

On the other hand, the difference of scale between thin conductors and the large dimensions of the soil domain Ω in conjunction with the large difference between the conductivities of their materials is known to pose a challenge to computations with the finite element method. In order to avoid the difficulties arising in this context, such as the large storage requirements for the mesh and the ill-conditioning of the resulting system of equations, the approach proposed in (SILVA et al., 2011) may be adopted.

In summary, the thin conductors are supposed to behave as perfect con-

ductors and are represented by lines in the geometrical model subjected to discretization. As discussed in the previous reference, if the volume of a thin conductor is omitted from the representation and is instead represented by a line, the sizes of the elements in its immediate vicinity result strongly related to the actual thin electrode radius. The setting of a suitable grid size in this region is then employed to recall the proper cross section of the thin conductor. This task may be addressed during the mesh generation step.

Additionally, proper constraints are prescribed for the degrees of freedom linked to the lines representing the conductors. Current excitation by pre-computed I_k is accomplished by means of non-homogeneous Neummann conditions applied to boundaries Γ_{FP} shown in Figure 5, as discussed in section 3.3.1. These surfaces are made coincident with mesh nodes representing the input points of the filamentary conductors by a limiting procedure (SILVA, 2006; SILVA et al., 2007). The perfect conductor behavior for the electrodes is obtained by a floating condition enforced on its nodal degrees of freedom (i.e. φ_i constant for every node along the line composing the filamentary conductor). In the case of the $\mathbf{A} - \varphi$ formulation arising from (3.23), a null value for edge-related degrees of freedom a_i is imposed along the conductor as well (SILVA, 2006; SILVA et al., 2007).

3.7 Chapter summary

This chapter presented the problem of conductive coupling phenomena taking place in the vicinities of a power system. The characteristics intrinsic to this class of applications that hinder its statement as a boundary value problem in a finite and closed domain were emphasized and were shown to be connected with the presence of multiple sites of current injection in the ground.

A procedure to compute a boundary condition for a truncated three-dimensional boundary value problem representing a zone where conductive coupling phenomena take place was then proposed by analyzing the analytical solutions of selected grounding arrangements. The proposed scheme consists in evaluating the electric potential at the underground boundary of the domain by means of the superposition of the effects of point current sources replacing the grounding electrodes actively injecting current in the ground. The potentials obtained can then be employed as a non-homogeneous Dirichlet boundary condition that can be incorporated in the finite element analysis of the corresponding problem.

In the following chapter, several problems will be analyzed with the aid of the technique proposed. The formulations of the finite element method pointed out in section 3.6 and their specializations will be adopted in conjunction with the boundary condition just proposed. The limitations of this approach and its applicability to more complex problems will be investigated as well.

4 CONDUCTIVE COUPLING APPLICATIONS

4.1 Introduction

In the previous chapter, the finite element analysis of conductive coupling phenomena with the use of a special boundary condition was proposed. This chapter now proceeds to the application of this technique.

According to section 3.5, the boundary condition procedure was derived by induction from an assortment of analytical problems. As a consequence, the assumptions adopted are expected to reflect into limitations affecting the general applicability of the technique.

These assumptions will be made explicit and discussed in this chapter. Some preliminary numerical problems will be proposed, in order to verify their validity in general applications.

Once the impact of those limitations is identified, the discussion will move on to the application of the technique to a more realistic situation. An actual transmission line right of way will then be analyzed, so as to show the capabilities of this approach.

It should be remarked that a significant part of the developments covered in this chapter has been published in recent journals and conference proceedings (MARTINHO et al., 2011; MARTINHO et al., 2014; MARTINHO; SILVA, 2015). This chapter then provides a compilation of these results in a more direct and logical

presentation.

4.2 Implicit assumptions and other general remarks

The boundary condition on the electric potential given by (3.21) relies upon the asymptotic behavior of the response exhibited by a point current source in steady state at far away distances. It also bears a conceptual dependence upon the principle of superposition of effects and on a hypothesis of homogeneous soil.

In finite element applications, the fulfillment of these assumptions are related to the following aspects:

- Computational domain Ω is made sufficiently large.
- The eventual existence of buried structures or heterogeneities in the soil does not disturb the distribution of the electric potential at large distances.
- All media involved exhibit linear behavior.
- The time variations of the sources are consistent with a steady state approximation.

The first two assumptions will be directly investigated in the following two sections. Both the influence of the size of the computational domain and the impact of buried structures will be examined in detail by means of the analysis of a series of specially conceived conceptual problems. A third section discussing a problem designed to show the advantage of the proposed technique in comparison with standard procedures for the finite element analysis with an open boundary is also included.

The strict satisfaction of the last two remaining aspects previously listed requires the introduction of simplifications or a restriction on the scope of application. For instance, the linear behavior of materials can only be ensured if effects such as the ferromagnetism of metallic structures or the soil ionization under intense surge currents are disregarded. Additionally, the steady state approximation is incompatible with phenomena characterized by fast rates of change, such as the current injection from a lightning discharge or the transients resulting from switching operations in the power system.

In face of these limitations, the problems analyzed in this chapter will tacitly assume the fulfillment of these two particular assumptions by considering simple materials and the flow of currents with the characteristic frequency of the power system (i.e. 60 Hz). It should be remarked, though, that a relaxation of these limitations and the use of concepts similar to the approach here proposed have also been considered by other authors in extended contexts of applications. For instance, (STOLL; CHEN; PILLING, 2004) also assumes a 1-D behavior of the fields beyond the truncation of the 3-D domain to compute the high-frequency impedance of grounding electrodes by the Finite Difference Method.

The last problem to be analyzed in this chapter is dedicated to a more realistic situation involving several buried structures and concerned with the investigation of the shielding effect produced by reinforcement bars sometimes contained within constructions.

All the numerical solutions obtained in this chapter were produced according to the techniques outlined in section 3.6, with software implementations that could be classified as experimental or non-optimized. In this sense, no attempt to exhaust the discussion of performance aspects of the numerical solutions is undertaken. Alternatively, the goal of this chapter is to lay the groundwork for

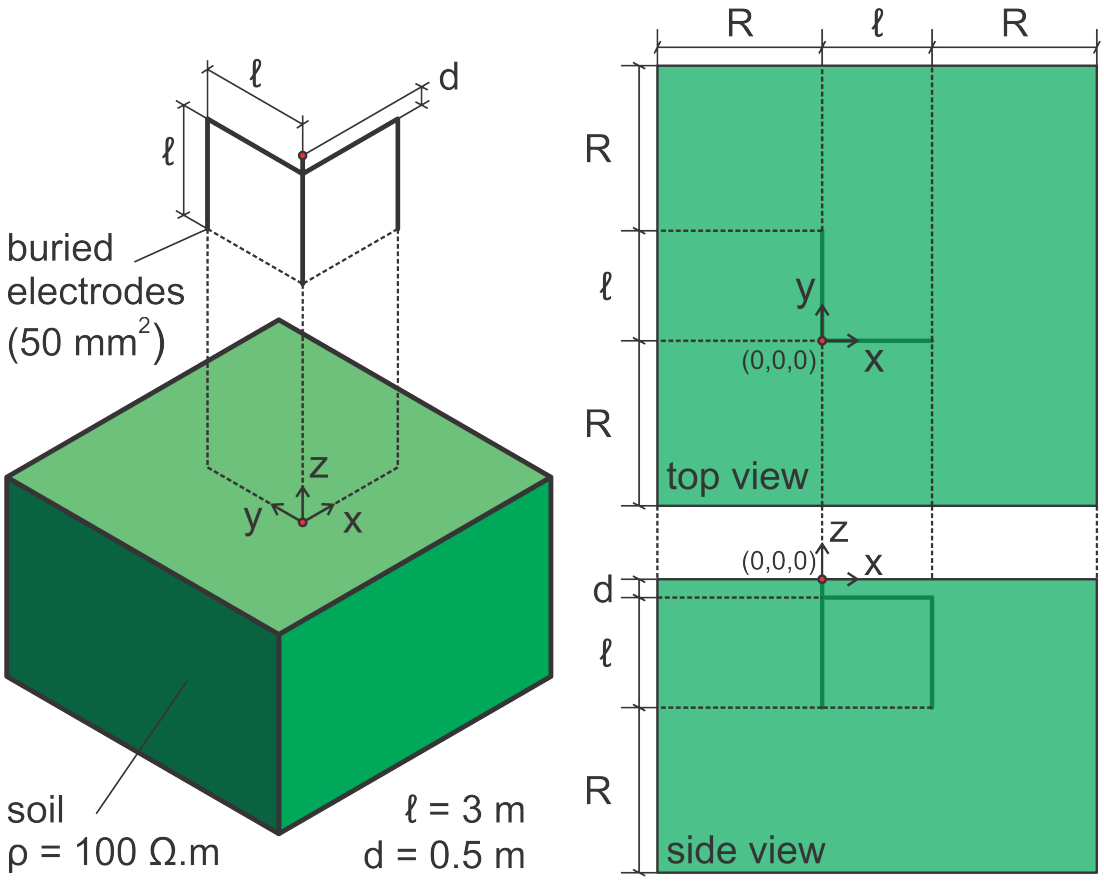

Figure 12: The grounding system under analysis and the parameterized domain for FEM computations.

future investigations in the numerical analysis of conductive coupling problems with the finite element method (FEM).

4.3 Domain size and superposition of multiple sources

The first configuration to be analyzed is shown in Figure 12 (MARTINHO et al., 2011). Several computations involving this configuration were carried out in order to establish a criterion for the dimensioning of the computational domain.

The grounding configuration represented in Figure 12 is composed of the interconnection of three vertical rods, and the ensemble is subjected to a fault current of $1\,\mathrm{A}$ and $60\,\mathrm{Hz}$. Current injection takes place at point (0,0,0) in ac-

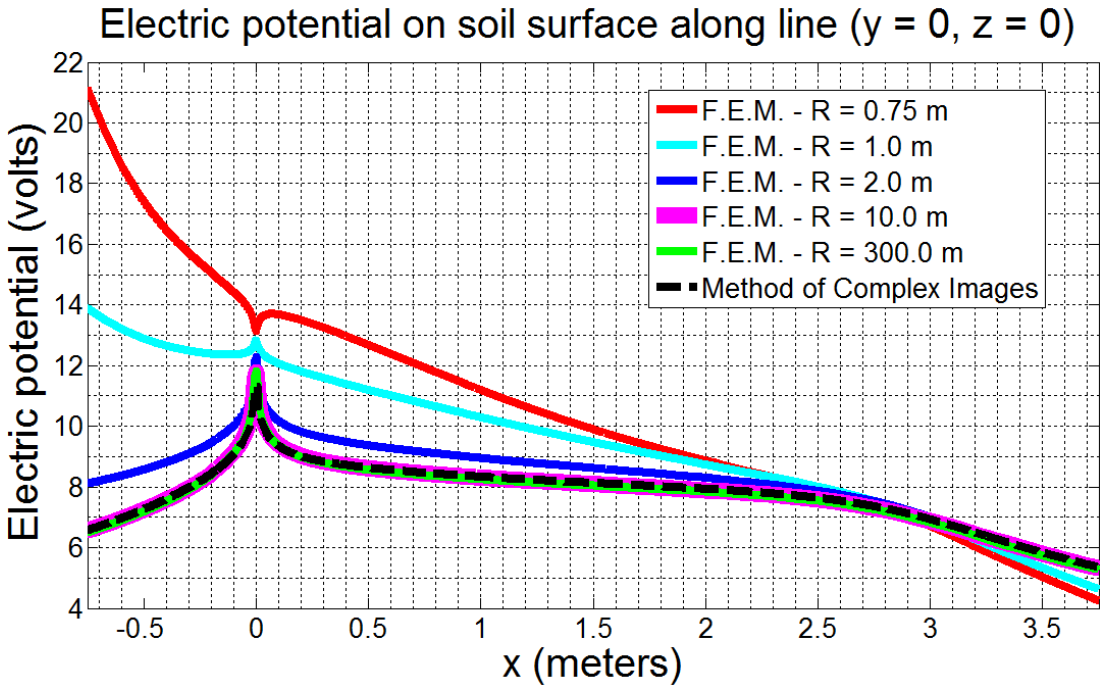

Figure 13: Earth surface electric potential for various values of parameter R with the FEM and for the MCI.

cordance with the system of coordinates attached to the representation. The $\mathbf{A} - \varphi$ formulation and the modeling approach for the electrodes described in sections 3.6.2 and 3.6.3 were adopted.

The investigation is based on a parameterization of the computational domain in terms of dimension R, which is also depicted in Figure 12. Several finite element method simulations were executed with different values of this geometrical parameter R. The aim is to verify the influence of the domain size on the validity of the point source approximation for calculating the non-homogeneous Dirichlet boundary conditions on the electric potential.

The results were compared with the solution given by the Method of Complex Images (MCI) (FILHO; CARDOSO, 1999; CHOW; YANG; SRIVASTAVA, 1992), an integral method that does not rely on domain discretization or truncation. The behaviors of the electric potential along the line ($y = 0$, $z = 0$) on the soil surface were plotted together in Figure 13 for comparison.

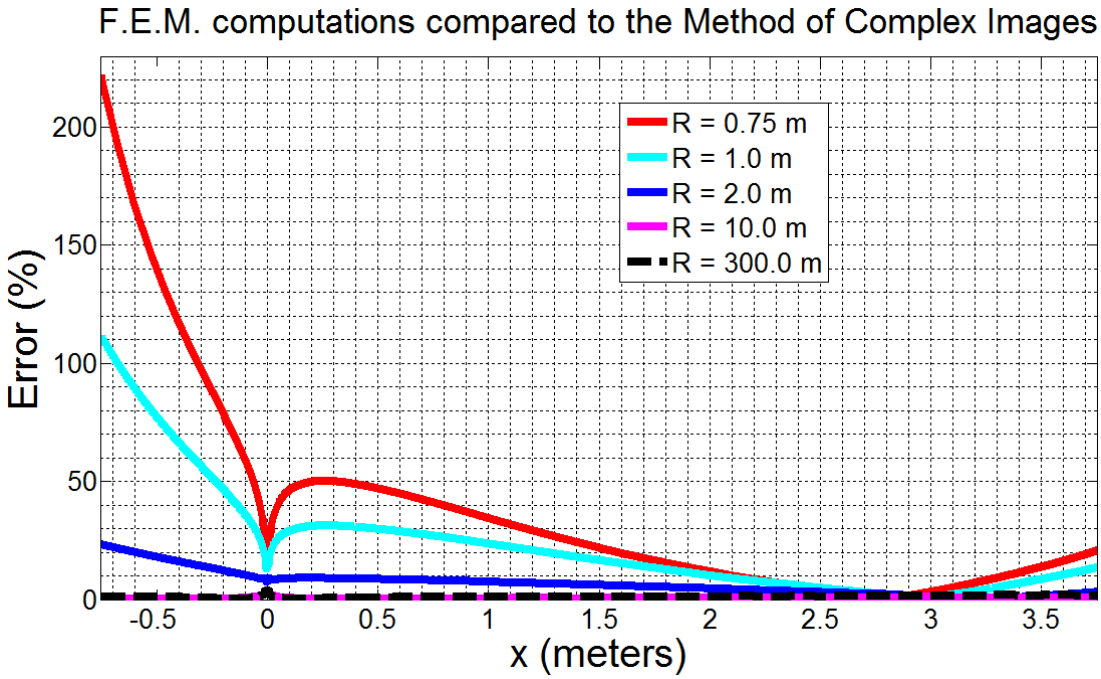

Figure 14: Error on the earth electric potential in comparison with the MCI.

Figure 13 shows that for sufficiently large domains the point source approximation leads to results in very good agreement with the MCI. Figure 14 displays the error in the electric potential of each FEM simulation compared to this reference solution along the same path. For the cases in which $R = 10\,\mathrm{m}$ and $R = 300\,\mathrm{m}$, errors lower than 4.5% were verified.

Greater insight into the effect of increasing the domain dimensions can be achieved with the aid of the sequence of plots composed of parts (a), (b) and (c) of Figure 15. These illustrations show the electric potential on the soil surface for increasing values of R, when the proposed non-homogeneous boundary condition is employed together with the $\mathbf{A} - \varphi$ formulation of the FEM in the modeling.

The computation for $R = 1\,\mathrm{m}$ on Figure 15(a) clearly shows that the domain is too small for the point source approximation to be applicable. It leads to a non-physical solution in which the electric potentials on the boundary may be larger than the ground potential rise at the injection point (0,0,0). However, if a

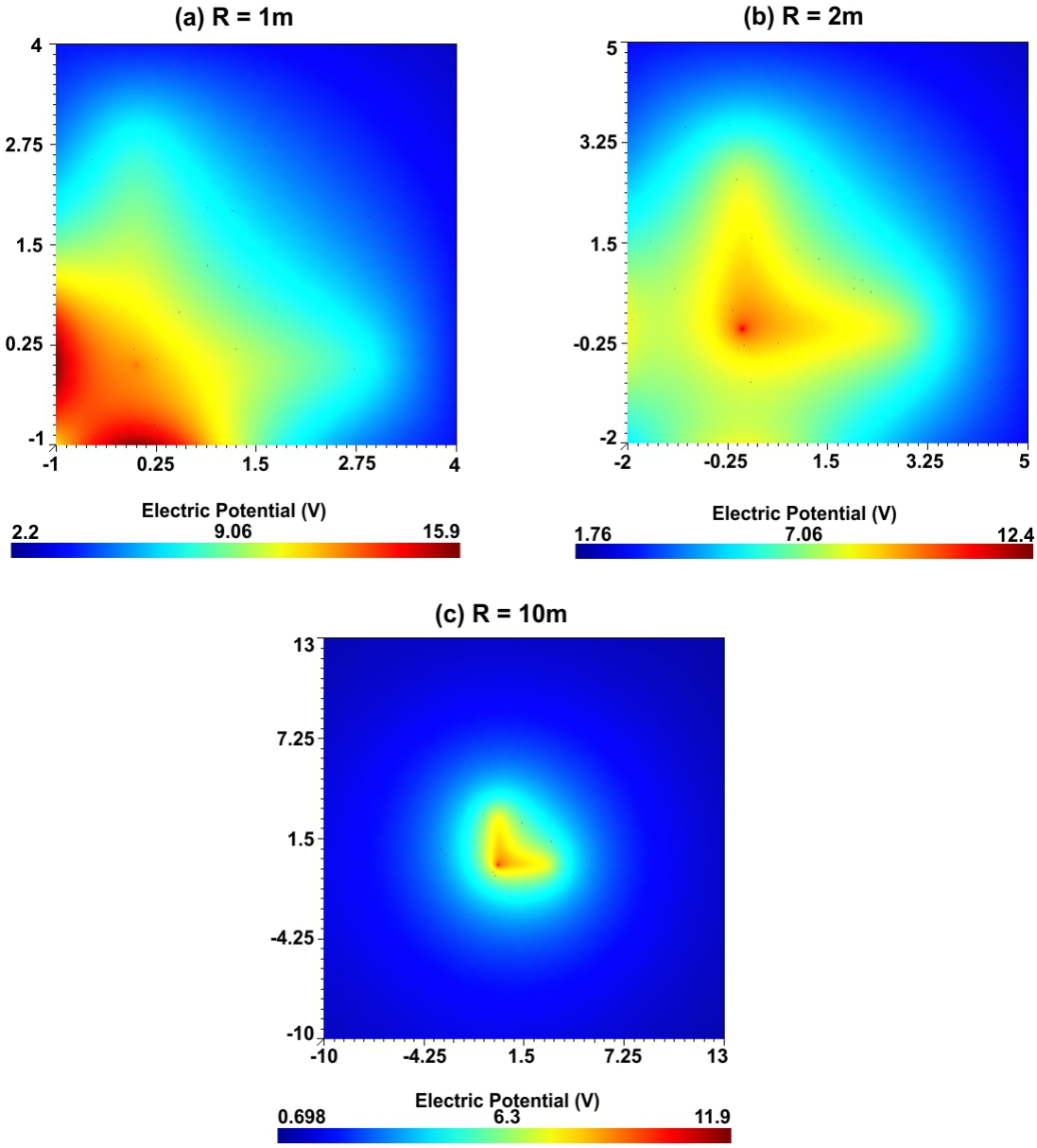

Figure 15: The behavior of the electric potential on the soil surface for different values of parameter R. Coordinates on each plot are measured in meters.

sufficiently large domain is employed, the electric potential solution accommodates itself into its expected distribution. This is the case in Figure 15(c).

Since the problem contained only a secluded grounding system, the application of the non-homogeneous boundary condition did not involve the superposition of multiple point current sources. In other words, the sum (3.21) contains only one term. Let then a second problem be considered in which two different grounding arrangements coexist in a limited space, as shown in

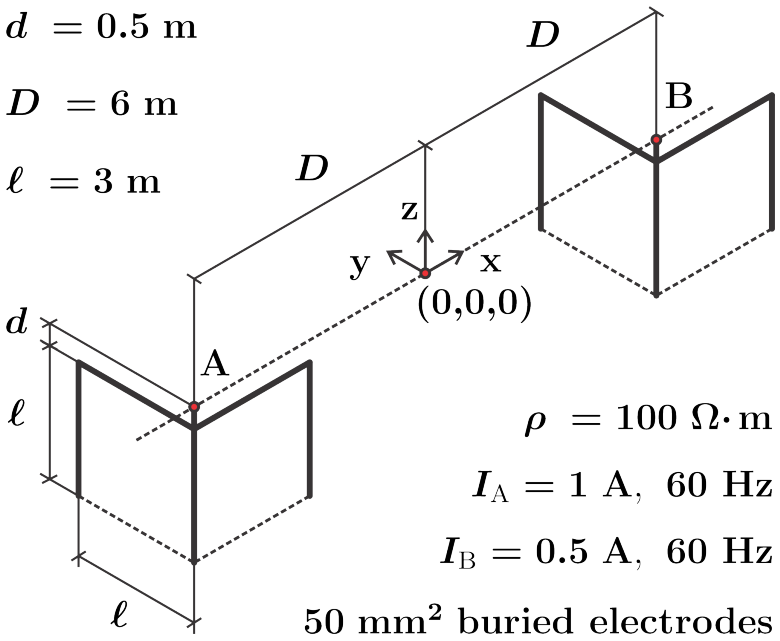

Figure 16: Two sets of vertically buried electrodes. The soil was omitted for clarity.

Figure 16 (MARTINHO et al., 2014).

In this new case, the same configuration of Figure 12 was repeated at a position $2D = 12\,\mathrm{m}$ away. The two resulting arrangements are labeled “A” and “B”. Grounding system A was once again subjected to a current of $1\,\mathrm{A}$ and $60\,\mathrm{Hz}$, while grounding system B received half of this current injection. A geometrical representation in which the truncation boundary (i.e. the Dirichlet boundary Γ_D) was approximately $20D$ away from the electrodes (or 10 times the separation $2D$ between the two grounding arrangements) was employed in the FEM solution.

The electric potential on the soil surface along line ($y = 0$, $z = 0$) was evaluated with the $\mathbf{A}-\varphi$ FEM formulation together with the proposed boundary condition. The results were plotted with the corresponding MCI solution in a single Cartesian plane, as shown in Figure 17. Errors no greater than 2.75% were verified.

It becomes evident from Figures 13 to 17 that the proposed boundary con-

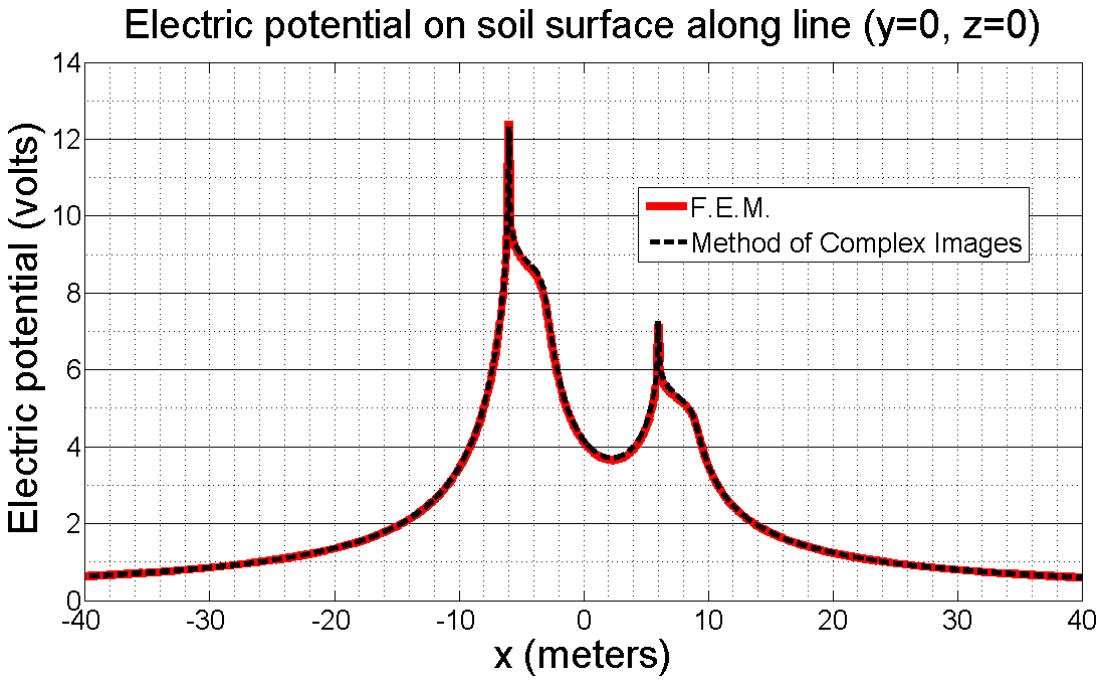

Figure 17: Earth surface electric potential for two grounding systems close to each other and subjected to unevenly distributed fault currents.

dition is valid only if the truncation boundary is placed at a sufficiently large distance from the sources. The results collected from the two problems previously analyzed suggest that Γ_D should be placed at distances a few times larger than a characteristic dimension of the conductive coupling problem under analysis.

The characteristic dimension for determining the domain size could be taken as either the length ℓ of an individual rod or the separation $2D$ between the two grounding arrangements. This information should be used with care by the analyst to avoid non-physical solutions (in the case of sub-dimensioned domains) or excessively large computational problems (in the case of over-dimensioning).

4.4 Effects of buried objects

The investigation conducted in the previous section addressed the appropriate dimensioning of the computational domain that is required by the non-homogeneous Dirichlet boundary condition (NHDBC) approach. This section now proposes an additional investigation, in order to verify the applicability of the alternative NHDBC in situations that do not fulfill another of the basic assumptions implied in its use.

More specifically, and as already mentioned, a hypothesis of homogeneous and isotropic soil is implicit in (3.21). As a consequence, some error should be expected when the NHDBC is employed in the analysis of conductive coupling problems containing additional structures embedded in soil domain Ω. Since the existence of underground heterogeneities at shallow depths is quite frequent in transmission line rights of way (as is the case of pipelines, valve boxes or masonry structures), a simplified problem following these lines will now be analyzed and discussed in detail (MARTINHO; SILVA, 2015).

The configuration in Figure 18 shows a vertical grounding rod similar to the one considered in section 3.4.3 subjected to a fault current. Two buried structures (a short box and a long cylinder) of the same material are placed in its vicinities. The xy plane cuts both the cylinder and the box in two equal parts. The relevant dimensions are indicated in Figure 18, along with the various physical properties.

The electric potential on the soil surface was computed along the x axis with two different approaches to truncate the domain: the NHDBC and infinite elements in a scheme analogous to the one represented in Figure 7. For the sake of convenience, both approaches were implemented for an electrokinetic formulation of the FEM.

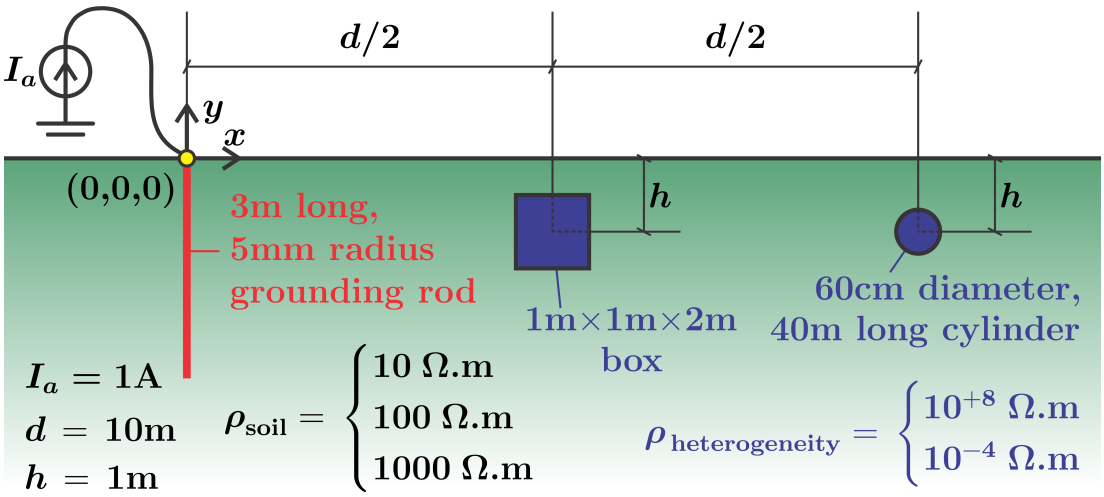

Figure 18: Configuration to investigate the effects of soil heterogeneities (represented by the buried structures in blue) on the behavior of the NHDBC approach. The resistivity values considered for the soil and for the underground structures are displayed above.

According to section 3.3.2, the infinite element technique is a well-established procedure for modeling open boundaries in finite element analysis. Its use relies on a modification of the Jacobian matrices of a layer of elements placed in the outermost boundaries of the domain. These adapted Jacobian matrices correspond to a transformation of coordinates that effectively map the geometrical finite elements of that special region into a particular reference element that extends itself to infinity. The use of this Jacobian matrix during the numerical integration of the local finite element matrices in conjunction with a homogeneous Dirichlet boundary condition for the electric potential on truncation boundary Γ_D results in the emulation of an open domain (DHATT; TOUZOT; LEFRANÇOIS, 2007; ZIENKIEWICZ; TAYLOR; ZHU, 2006).

The problem under analysis is not affected by a neglect of additional current sources left outside the computational domain, as discussed in section 3.3.2. Therefore, the finite element analysis with the infinite element technique is taken as the benchmark for validating the NHDBC approach in the case of a soil with buried objects.

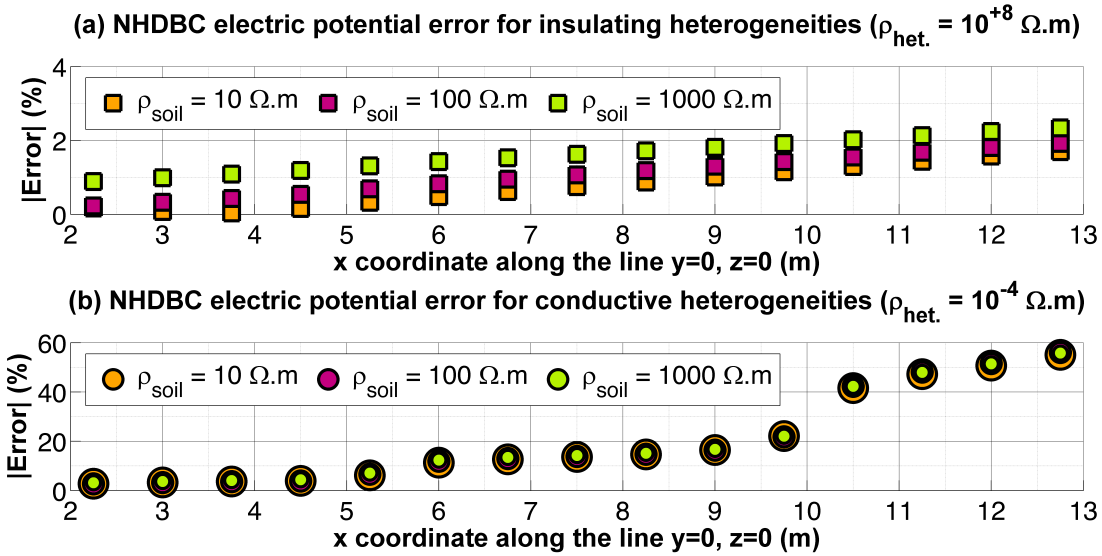

Figure 19: Comparison of the NHDBC approach with the use of infinite elements in the investigation of the effects of soil heterogeneities.

The errors in the electric potential for the NHDBC solution to the reference solution were evaluated along the x axis for different combinations of soil and heterogeneities resistivities. The graphs in Figure 19 keep the same system of coordinates of Figure 18 and present the results for the region immediately above the buried heterogeneities on the soil surface. The plot depicted in Figure 19(a) displays the percent error of the NHDBC approach for the case of insulating heterogeneities, when compared with the corresponding solution obtained with infinite elements. Figure 19(b) makes the same comparison for the case of conductive heterogeneities.

The following conclusions arise from the data expressed by the plots of Figure 19:

- For a wide range of soil resistivities, the NHDBC approach is still very accurate if highly resistive objects are embedded in the soil. A maximum error below 2.4% for $\rho_{soil} = 1000\ \Omega.m$ was verified.

- When highly conductive heterogeneities are considered, significant errors are verified in the surface electric potential distribution computed

Table 1: Performance of the System of Equations Solver[†] (Insulating buried objects)

Soil resistivity	NHDBC solution[‡]	ZIEs solution[‡]
$10\ \Omega$.m	304	340
$100\ \Omega$.m	292	336
$1000\ \Omega$.m	304	326

[†] BiCGStab, Jacobi preconditioning, tolerance = 10^{-5}.
[‡] Number of iterations to achieve convergence.

with the NHDBC approach.

- If heterogeneities of intermediate resistivity are considered, the NHDBC approach may also be very accurate. This will still be the case when their resistivities are in a range that is not far from the resistivity of the surrounding medium. The situation would correspond to practically no heterogeneities.

The results of Figure 19 were obtained with a mesh of tetrahedra and prisms, composed of 37224 nodes. The system of equations could have been solved with any appropriate method, and the BiCGStab algorithm was chosen for convenience. Comparative information about its performance is available in Table 1, for the case of insulating heterogeneities in which both techniques provide similar solutions for the electric potential distribution. It may be verified that the NHDBC technique led to a slightly smaller computational effort.

4.5 Effects of external currents

The motivation for introducing an alternative approach for dealing with a semi-infinite domain in the context of conductive coupling problems involving overhead lines was discussed in section 3.3.2. It was argued that the widespread techniques employed in addressing this category of problem with the finite element method would inevitably neglect the effects of current injec-

tion sites left outside the computational domain.

It may be shown that this neglect leads to a significant error in the electric potential computed on the earth surface, which is one of the most relevant physical quantities in this kind of investigation. However, one may verify that better results can be obtained if the NHDBC is applied instead.

To make these assertions explicit, let the configuration of Figure 20 be considered, in which two neighboring vertical grounding rods are represented (MARTINHO; SILVA, 2015).

The soil is supposed to be homogeneous and the rods are subjected to two independent current sources. A full, rigorous electrokinetic FEM model would contain both rods embedded in a semi-infinite soil domain, represented by a layer of infinite elements, as shown in Figure 20(a). Solutions for the electric potential distribution following from this approach will be quoted from now on as being produced by the “complete” model.

Still, if a detailed analysis of the potential distribution must be limited only to the vicinities of the first grounding rod, a simplified representation could be proposed as well, as depicted in Figure 20(b). This model neglects the existence of the second grounding rod and the soil is also taken as a semi-infinite domain truncated by infinite elements. In opposition to the “complete” approach previously defined, this model will be referred to as the “reduced” one.

The reduced model is conceived in the likeness of the scenario recovered in the beginning of this section, which arises in the modeling of a complex conductive coupling situation with any standard technique dedicated to treating the open boundary that forces the neglect of field sources left outside the computational domain.

The application of the NHDBC scheme to the problem under analysis yields

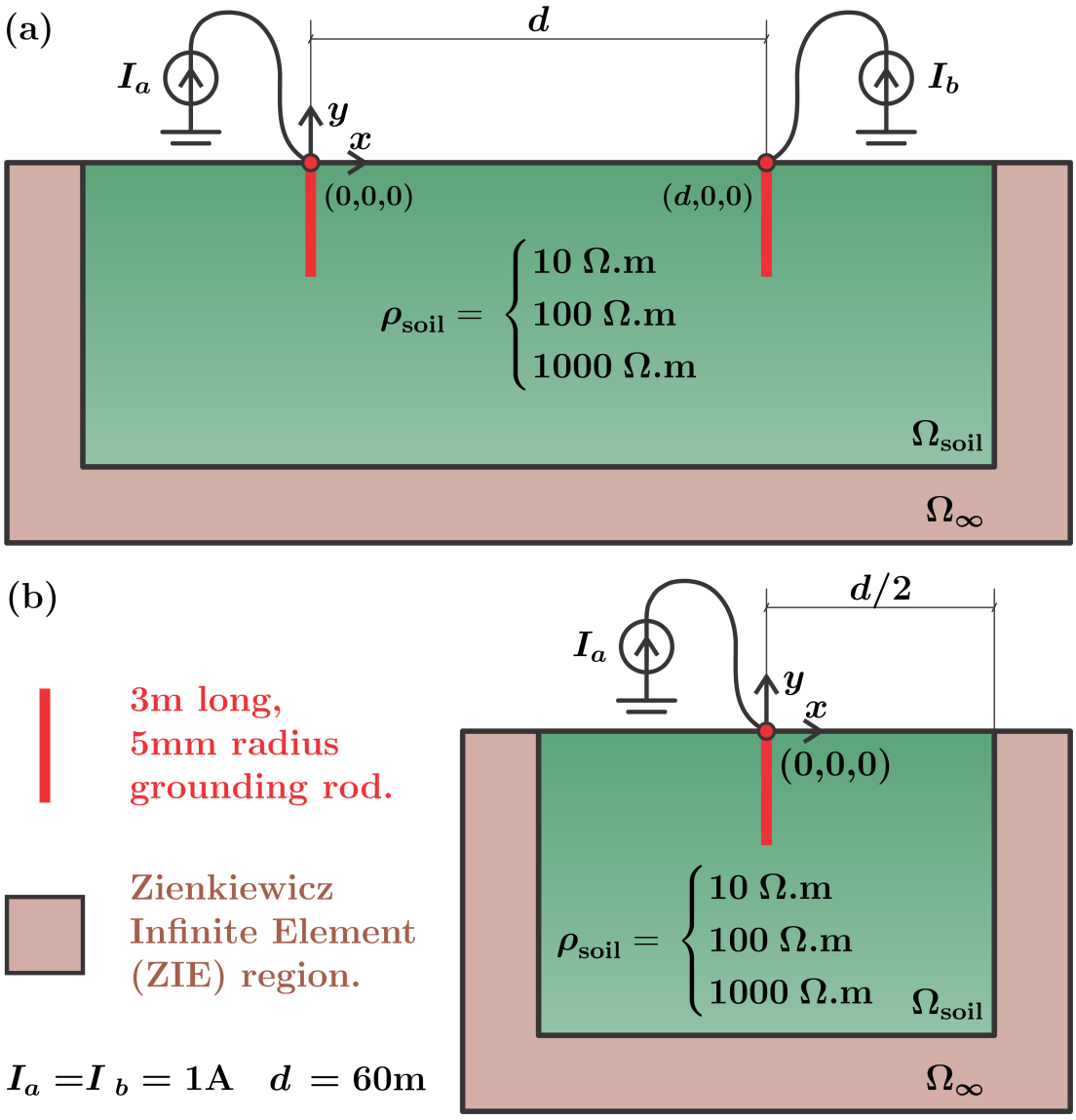

Figure 20: The complete (a) and reduced (b) models for the FEA of the problem of two neighboring grounding rods.

the situation depicted in Figure 21. Here, the second grounding rod, which lies outside the computational domain, is taken into account by means of an additional point source in the summation given by (3.22), as would be the case for the grounding grids of nearby transmission line towers in a right of way.

In order to compare this third approach with the well-established procedure given by the reduced model, the electric potential distribution provided by the complete model solution was fixed as a benchmark. The plot on Figure 22 thereby displays the behavior of the percent error in the electric potential be-

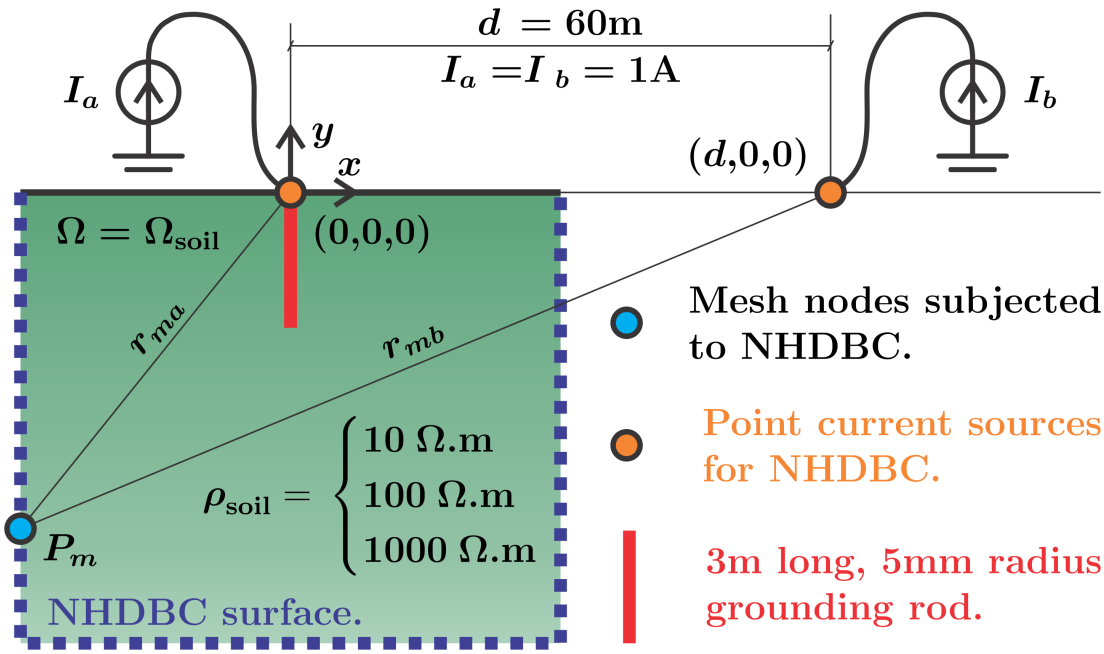

Figure 21: The NHDBC applied to the problem of two neighbouring grounding rods.

tween both the reduced and the NHDBC solutions and this reference. These errors were evaluated along the x axis in the vicinities of the first grounding rod, with several soil resistivities. The system of coordinates, the relevant geometrical parameters and the material properties employed in the simulations are shown in Figures 20 and 21.

The following may be derived from Figure 22:

- Both the NHDBC and the reduced model yield low errors ($\leq 0.7\%$ in all cases) for the ground potential rise at the point of current injection. Hence, if only the equivalent grounding resistance during the fault is required, the two approaches provide equivalent results.

- If only positions located at distances of the order of a few times the rod length ($\ell = 3\,\text{m}$) are concerned ($|x| \leq 4\ell = 12\,\text{m}$), the NHDBC still provides small errors ($\leq 6.65\%$) for the electric potential. This is not the case for the reduced model, which yields much larger errors ($\leq 26.2\%$).

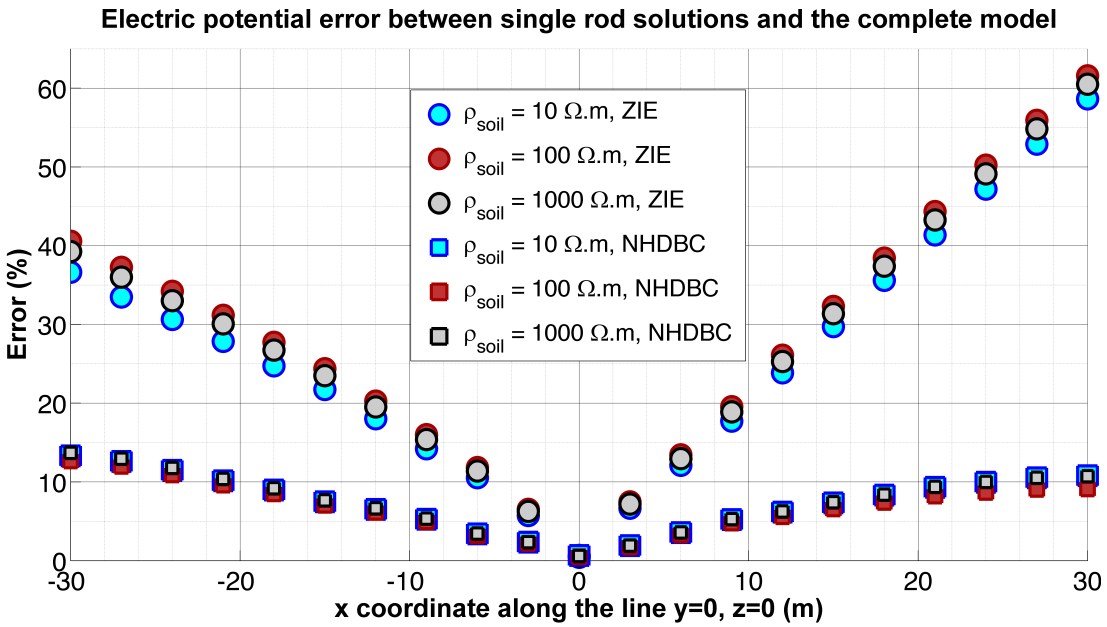

Figure 22: Comparison of the NHDBC and reduced approaches with the complete model for various values of soil resistivities (rod position: $x = 0$ m).

- The outskirts of the domain should be interpreted as a region lying halfway to relevant structures left outside the computational domain (as is the second grounding rod at $x = 60$ m). In this sense, they should be preferably analyzed with the complete model. However, even in this unfavorable region for both single rod approaches, the NHDBC procedure yields smaller errors than the reduced model. At the border of the computational domain the closest to the second grounding rod ($x = 30$ m), the former leads to errors no greater than 11%, while the latter yields an unacceptable error of almost 62%.

A similar behavior with results even more favorable to the use of the NHDBC is verified when the same investigation is repeated for a path along the z axis. It may be concluded then that the NHDBC technique provides a better modeling approach for the problem of Figure 20. Ultimately, the facts previously made explicit also suggest that similar results would also be verified in more realistic conductive coupling problems, possibly involving other faulted

transmission line towers and their grounding networks.

4.6 Application to a conductive coupling problem in a transmission line right of way

In this section, a realistic application will be considered (MARTINHO et al., 2014). The configuration under analysis is depicted in Figure 23. It shows the surroundings of an area spanned by two towers of a transmission line close to an underground pipeline section, which is made accessible to working personnel inside a steel-reinforced masonry structure. The ground networks of the towers have a particular configuration given by long conductors buried in a direction parallel to the overhead line, which is sometimes called counterpoise grounding.

The power system is supposed to be subjected to a fault that results in the injection of components of power frequency current at the foundation of each tower by the mechanism discussed in section 3.2. Their values are known in advance from a previous system-wide computation, and are available together with other relevant data in Figure 23.

The pipeline is buried at a depth of 1.04 m and the masonry structure has the shape of a box with dimensions $4.0\,\mathrm{m} \times 3.35\,\mathrm{m} \times 2.4\,\mathrm{m}$. It should be remarked that the pipeline is represented by a cylinder entirely composed of a very resistive material, as is the case of the coatings normally employed for protecting their metallic structures. This simplification together with the other resistivity values employed (available in Figure 23) lead to a model in accordance with the conclusions of section 4.4, as required for using the NHDBC approach.

The aim of this problem is to investigate the mitigatory role played by the

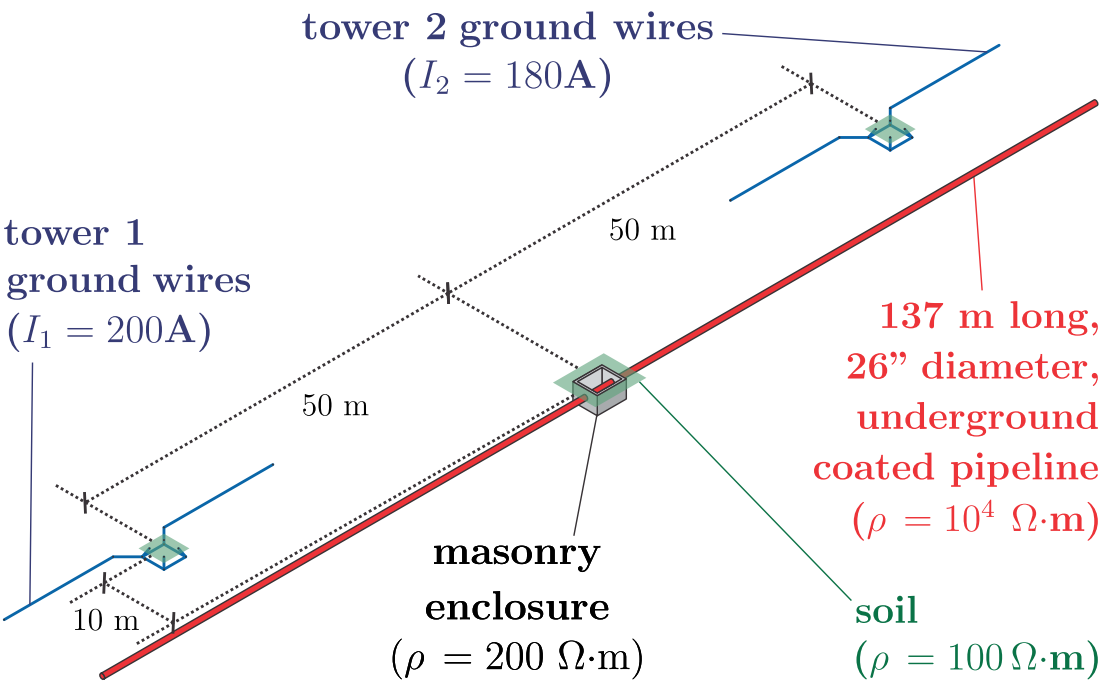

Figure 23: Underground structures sharing the transmission line right of way.

embedded steel reinforcements, that is, their ability to modify the electric potential distribution next to the working area and to lessen both touch and step voltages during the contingency.

The problem was solved with the $\mathbf{A} - \varphi$ edge formulation. Both the steel reinforcements and the grounding networks were modeled with the aid of the floating boundary condition technique outlined in section 3.6.3. Thus, a geometric model for the right of way represented in Figure 23 was created in compliance with the dimensioning orientations established in section 4.3 and discretized with a mesh of tetrahedra (with 4 nodes and 6 edges per tetrahedron).

The application of the complete numerical scheme previously described to this model yielded an algebraic system of equations with approximately $2\,200\,000$ degrees of freedom. The solution of this system provided the electric potential distribution in domain Ω.

Figure 24 shows a general view of the computational domain after the so-

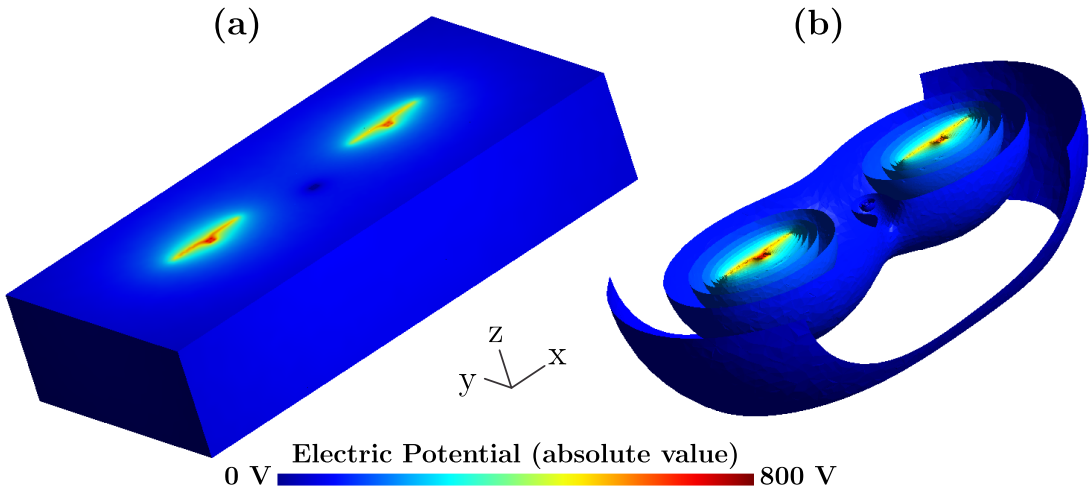

Figure 24: Overview of the solution (a) and its equipotential surfaces (b).

lution and the equipotential surfaces of the electric potential distribution. Figure 25 displays the electric potential on the soil surface in the surroundings of tower 2. The information given by this plot could be employed to evaluate step voltages for this region of the transmission line right of way.

The investigation of the mitigatory effect of steel reinforcement bars is accomplished with the aid of Figure 26, in which a detail of the enclosure is shown. Table 2 brings the results for touch voltages for three enclosure con-

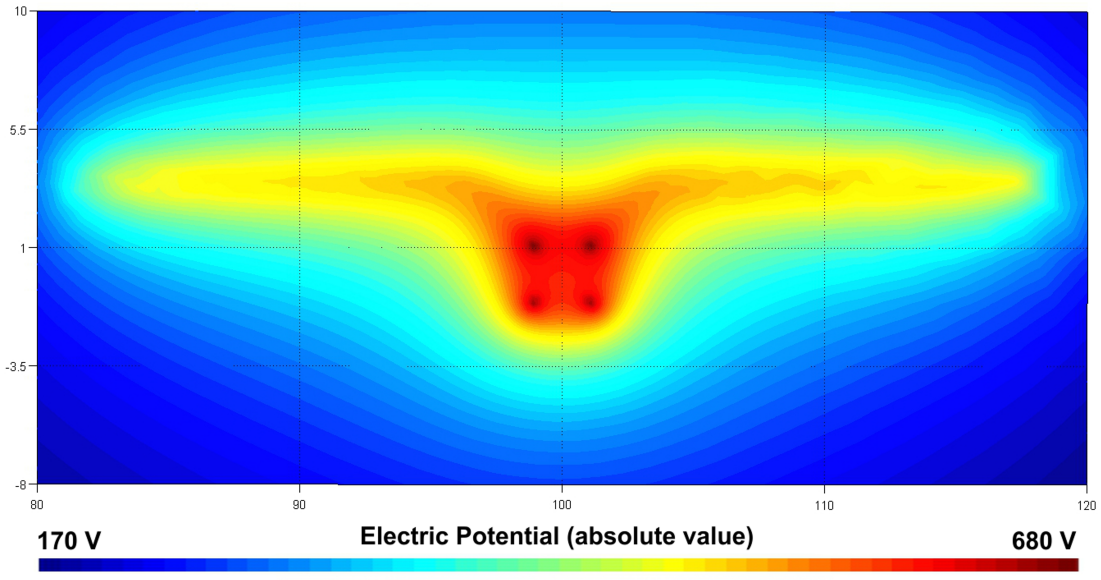

Figure 25: Electric potential on the earth surface in the neighborhood of tower 2 (position coordinates measured in meters).

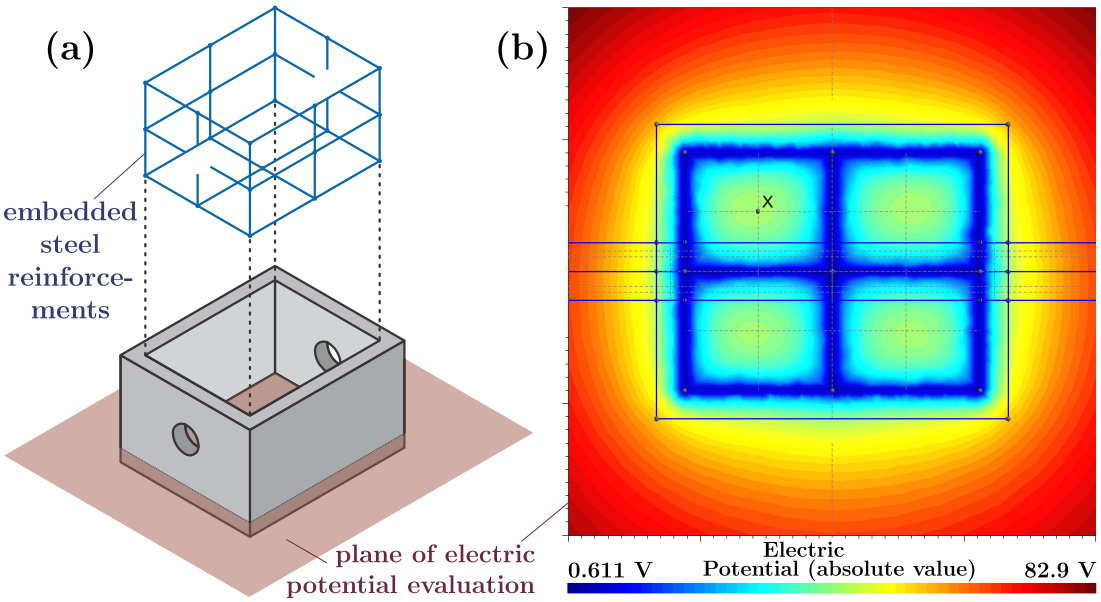

Figure 26: Detail of the masonry enclosure (a) and the plane of electric potential evaluation (b).

Table 2: Touch Potential Inside the Masonry Enclosure

Reinforcements configuration	Touch Potential†
Corners and inner walls‡	42.9 V
Inner corners only	58.7 V
No reinforcements	122.0 V

† For a subject stepping on the spot marked with an X in Figure 26(b) and touching a perfectly grounded structure at 0 V.
‡ As depicted in Figure 26(a).

figurations, which differ from each other in the distribution and presence of embedded steel reinforcement bars.

The results gathered in Table 2 confirm the expected influence of the steel reinforcement bars, that is, their ability to lessen dangerous overvoltages in the working area. The touch voltages quantified with the numerical scheme described herein could then be considered for safety measures, or could be employed in the project or design of a shared transmission line right of way.

4.7 Chapter summary

This chapter presented a series of conductive coupling problems analyzed with the FEM and the NHDBC. The limiting assumptions brought by the use of this approach were analyzed by solving two test problems. The results allowed ascertaining directives concerning the size of the computational domain and provided the ground rules for determining the nature of the heterogeneities buried in the soil that are compatible with the use of this technique.

A complementary test problem was analyzed as well, in order to confirm the need of an alternative procedure such as the NHDBC to circumvent the difficulties pointed out in section 3.3.2, which result from the use of conventional modeling techniques for representing domains with open boundaries. The same analysis showed that the use of the NHDBC approach can be advantageous in this context of conductive coupling applications.

Finally, a more practical conductive coupling application was considered, in which the shielding effect provided by reinforcement bars embedded in a buried masonry enclosure was simulated by means of a large-scale FEM computation. This application illustrated the modeling possibilities granted by the use of the NHDBC approach.

In the case of the preliminary applications of the proposed technique, the validation of the computed results was obtained by confrontation with alternative numerical techniques. According to the case, the method of complex images or the finite element method with the infinite element technique were chosen as benchmark solutions.

Ideally, the validation of the results should also be carried out in the case of section 4.6 by comparing them with measurements. However, the setting up for the experimental validation of conductive coupling applications involving

high voltage power systems corresponds to an elaborate enterprise and is far beyond the scope of the current work.

The investigation of additional practical conductive coupling problems and further research on numerical aspects of finite element solutions employing the NHDBC approach are left for future works.

5 INDUCTIVE COUPLING MODELING AND APPLICATION

5.1 Introduction

In the two previous chapters, conductive coupling phenomena were considered and analyzed with the finite element method. This chapter proceeds with the investigation of inductive coupling phenomena.

The inductive coupling between an overhead transmission line and other nearby structures arises from the time-varying magnetic field induced by the electric currents flowing in its conductors. If contingencies and transient conditions are disregarded, these currents vary with the power system frequency, which is either 50 Hz or 60 Hz depending on the national standard. In both cases the time variations are sufficiently slow to result in negligible capacitive and propagation effects.

On the other hand, these time rates of change are fast enough to yield relevant inductive phenomena. The electric field induced by the line time-varying magnetic field leads to an induced electric potential and to an induced current density that may be dangerous to humans or affect the stability of susceptible structures. The resulting undesired effects are manifold, ranging from the risk of electric shock to the continued alternate current corrosion of metallic structures (CENELEC, 2012; CENELEC, 2013).

The modeling of this class of problems can be attained with well-known nu-

merical procedures such as the FEM. In situations involving the parallelism of long structures with the transmission line, as is the case of transportation rails or underground pipelines, this method may be efficiently employed (CHRISTOFORIDIS; LABRIDIS; DOKOPOULOS, 2005). The shared right of way may be reduced to a representative 2-D model given by one of its cross-sections, leading to numerical problems of reasonable size and complexity, even if large inactive air regions and thin phase conductors need to be discretized.

The general problem is however given by an object of an arbitrary shape and with an arbitrary position relative to the transmission line. The finite element analysis of these problems requires a 3-D model. As a result, both the storage requirements and the computational run times associated to the numerical procedure tend to increase greatly, turning the discretization of inactive air regions and of thin conductors into heavy burdens that cannot be avoided with classical FEM formulations.

In face of these difficulties, an approach based on an integral method is proposed. More specifically, the use of an adapted version of the generalized Partial Element Equivalent Circuit (PEEC) integral method (NGUYEN et al., 2014) is considered.

Since the use of a PEEC-like method to model inductive coupling phenomena in transmission line rights of way is an unconventional application of this class of techniques, its formulation and the required adaptions will be covered in this chapter. The numerical procedure will then be applied to a problem involving two different orientations of an underground object subjected to the influence of an overhead line. The results will be confronted with solutions issued from the 2-D and 3-D FEM.

5.2 The generalized PEEC integral formulation

The generalized PEEC approach arises from a synthesis of concepts, namely the classic PEEC method (RUEHLI, 1974) and the approximation of field quantities of conservative flux by vector facet elements (BOSSAVIT, 1988).

The following subsections contain a fairly stand-alone presentation of this integral formulation. For additional details on the generalized PEEC method or on other related formulations, the reader is referred to (NGUYEN et al., 2014; NGUYEN, 2014).

5.2.1 Derivation of the PEEC integral equation

In accordance with section 1.3, electric field $\mathbf{E}$ may be written in terms of magnetic vector potential $\mathbf{A}$ and electric scalar potential φ. This statement is confirmed by (1.8), which is repeated below for convenience:

$$\mathbf{E} + \frac{\partial \mathbf{A}}{\partial t} = -\nabla\varphi. \tag{5.1}$$

In order to obtain the integral equation that establishes the basis of the PEEC procedure, the left-hand side of (5.1) must be recast in terms of current density $\mathbf{J}$. The connection between $\mathbf{E}$ and $\mathbf{J}$ in a medium of conductivity σ is given by Ohm's law, according to (1.4). The dependence between fields $\mathbf{A}$ and $\mathbf{J}$ is given by

$$\mathbf{A} = \frac{\mu_0}{4\pi} \int_{\Omega} \frac{\mathbf{J}}{r}\, \mathrm{d}\Omega. \tag{5.2}$$

In (5.2), Ω is a conductive domain containing the current density $\mathbf{J}$. Distance r is measured between the evaluation point for $\mathbf{A}$ and an element of volume $\mathrm{d}\Omega$. This expression neglects the time retardation of the magnetic vector potential (STRATTON, 2007; JACKSON, 1999), assuming quasi-static electro-

magnetic fields. Magnetizations and electric polarizations of the media are not taken into account.

From this point onwards, a sinusoidal time dependence with an angular frequency ω will be assumed. The time dependent fields then become complex quantities and the time derivative operator is substituted by $j\omega$. This said, the substitution of (1.4) and (5.2) into (5.1) gives rise to

$$\frac{\mathbf{J}}{\sigma} + \frac{\mu_0}{4\pi}\, j\omega \int_{\Omega} \frac{\mathbf{J}}{r}\, \mathrm{d}\Omega + \nabla\varphi = 0, \tag{5.3}$$

which is an integral equation relating the current density distribution and the electric potential in the frequency domain.

5.2.2 Finite element approximation of the current density field

Let conductive region Ω be now discretized with a mesh of finite elements in order to approximate the current density distribution. The interpolation scheme adopted is based on vector facet shape functions, to enforce the conservation of the current flowing between element interfaces.

Inside a finite element e, the current density is approximated by the linear combination of its facet shape functions $\mathbf{w}_j^e$ given by

$$\mathbf{J}^e = \sum_j \mathbf{w}_j^e\, I_j^e, \tag{5.4}$$

where j spans the total number of facets of the element and the I_j^e are unknown current values flowing through each facet. This physical meaning of the coefficients I_j^e comes from the basic property of the facet shape functions given by

$$\int_{\Gamma_i^e} \mathbf{w}_j^e \cdot \mathbf{n}\, \mathrm{d}\Gamma_i^e = \delta_{ij}, \tag{5.5}$$

where indexes i and j are associated to facets; $\mathbf{n}$ represents the outward nor-

mal vector of a facet Γ_i^e and δ_{ij} is the Kronecker delta.

The explicit analytical expressions $\mathbf{w}_j^e$ for the shape functions depend on the element type (tetrahedra, hexahedra, etc.) (DULAR et al., 1994). These vector shape functions are defined to be null outside their corresponding element e, that is, the shape functions from different elements are never overlapping.

This allows a global numbering of facets to be considered, so that the current density approximation in the whole of Ω may be simply expressed as

$$\mathbf{J} = \sum_j \mathbf{w}_j I_j, \tag{5.6}$$

where index j now spans all the facets from the discretization and where superscript e was dropped.

5.2.3 Galerkin projection

If (5.3) is rewritten in terms of the finite element approximation of the current density field given by (5.6), its left-hand side will not be exactly null. The following vector residual will be obtained instead:

$$\mathbf{R} = \frac{\sum_j \mathbf{w}_j I_j}{\sigma} + \frac{\mu_0}{4\pi} j\omega \int_\Omega \frac{\sum_j \mathbf{w}_j I_j}{r} \, \mathrm{d}\Omega + \nabla\varphi \neq 0. \tag{5.7}$$

A system of equations in terms of the set of unknown facet currents $\{I_j\}$ may be assembled by minimizing this residual, in the sense provided by the Galerkin method. The procedure consists in the computation of a set of weighted residuals $\mathcal{R}_i$, which are all set to zero. The weighting functions are taken from the set of vector facet shape functions $\{\mathbf{w}_i\}$ of the current density approximation in Ω:

$$\mathcal{R}_i = \int_\Omega \mathbf{R} \cdot \mathbf{w}_i \, \mathrm{d}\Omega = 0. \tag{5.8}$$

When taken together into account, the residuals $\mathcal{R}_i$ equaled to zero lead

to the aforementioned system of equation. This system acquires the following structure:

$$[Z] \cdot [I] = ([R] + j\omega [L]) \cdot [I] = [\Delta\varphi] . \tag{5.9}$$

In (5.9), $[I]$ is a column vector storing unknown facet currents I_j. The general entries of the other matrices in this system are:

$$R_{ij} = \int_{\Omega} \frac{\mathbf{w}_i \cdot \mathbf{w}_j}{\sigma} \, \mathrm{d}\Omega , \tag{5.10a}$$

$$L_{ij} = \frac{\mu_0}{4\pi} \int_{\Omega} \mathbf{w}_i \cdot \left(\int_{\Omega} \frac{\mathbf{w}_j}{r} \, \mathrm{d}\Omega \right) \mathrm{d}\Omega \quad \text{and} \tag{5.10b}$$

$$\Delta\varphi_i = - \int_{\Omega} \mathbf{w}_i \cdot \nabla\varphi \, \mathrm{d}\Omega. \tag{5.10c}$$

5.2.4 Circuit interpretation

The notation adopted for the matrices in (5.9) and their general terms in (5.10) suggest that an equivalent circuit may be proposed for the numerical procedure just described. This is indeed the case, and this circuit interpretation is obtained as follows:

- Each element in the finite element mesh is associated to a circuit node placed in its centroid; the centroids of each facet lying on the boundaries of Ω are associated to a circuit node as well.
- A facet i corresponds to a circuit branch of impedance $Z_{ii} = R_{ii} + j\omega L_{ii}$, calculated by (5.10a) and (5.10b) with $i = j$. This branch connects the two nodes associated to the two mesh elements sharing facet i.
- A circuit branch is coupled to every other branch of the circuit by means of a mutual inductance. The mutual inductance between a branch (or facet) i and a branch j is calculated by (5.10b) with $i \neq j$.

Additionally, the right hand-side of (5.9) may be shown to be a vector of av-

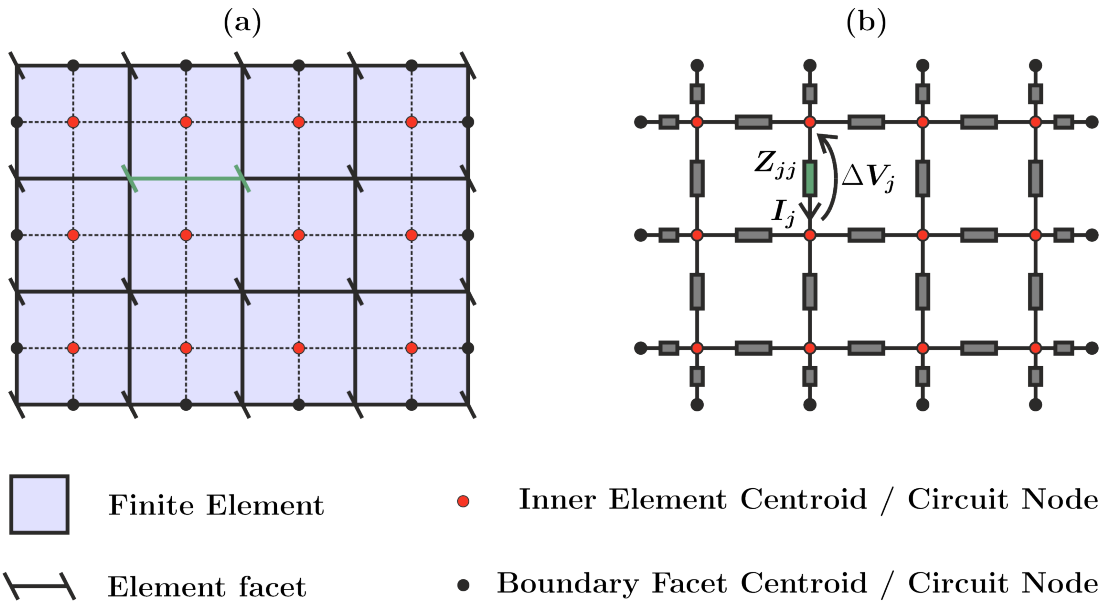

Figure 27: 2-D representation of the equivalence between the application of the PEEC formulation to a mesh of hexahedra (a) and an electric circuit (b). The mutual inductance couplings L_{ij} are omitted.

eraged branch (or facet) voltage drops (NGUYEN et al., 2014). More specifically, $\Delta\varphi_i$ calculated by (5.10c) gives the difference between the averaged electric potential φ of the two elements sharing facet i. For a facet lying on the border of the domain, the same computation gives the difference between the averaged electric potential of the only element containing the facet and the mean electric potential of the boundary facet itself.

Figure 27 illustrates this circuit equivalence, which also allows the use of electric circuit solver algorithms to solve the system of equations (5.9). The motivations for such an approach are the following:

- The use of facet elements assures the conservation of current between element interfaces. The use of an electrical circuit solver naturally enforces the conservation of current in the problem under analysis in a global sense. Together they assure the solenoidal character of current density field $\mathbf{J}$ predicted by (3.1), which follows from the neglect of displacement currents or capacitive effects.

- If the analysis is carried out by means of a circuit solver, the coupling of the electromagnetic equations to a complementary external network becomes straightforward. Interesting modeling possibilities arise from this fact, as will be clarified in the application that follows.

Note that the circuit equations (5.9) are stated in terms of unknown branch currents $[I]$. However, circuit solvers are conceived employing independent loop currents or nodal tensions as unknowns, not branch currents and voltage drops.

In this way, an independent loop search algorithm is employed to convert the problem given by (5.9) into a well-posed form for mesh current analysis (NGUYEN et al., 2012). Clearly a transformation from independent loop currents to branch currents is required after the solution of the equivalent electric circuit, to evaluate field quantities during the post-processing stage of the analysis.

5.2.5 Other numerical issues

The assembly of the system given by (5.9) involves the numerical integration of the terms given by (5.10a) and (5.10b) for every facet of the finite element mesh. These terms must be assembled to matrices $[R]$ and $[L]$ and stored efficiently. This section discusses some related issues that arise in the context of application of an integral method.

Matrix $[R]$ is sparse, since (5.10a) is non-zero only when i and j are facets belonging to the same mesh element. Thus, its terms are integrated and stored in a rather conventional way, as in a traditional FEM code. On the other hand, matrix $[L]$ is dense due to the mutual inductance coupling between every two branches of the equivalent network.

This feature of the PEEC inductance matrix is shared with other integral methods, and leads to some practical implementation difficulties that are addressed in the following paragraphs.

The numerical integration of expressions such as (5.10b) is costly from a computational point of view. These integrations need a large number of Gaussian quadrature points when compared to the numerical integration of a conventional finite element matrix. Moreover, in the former the Gaussian quadrature points must be chosen carefully, in order to prevent singularities of the term $G(r) = {}^{1}\!/\!_{r}$ from taking part in the integrand.

In addition, the assembly time of a dense matrix $[L]$ and the memory required for its storage tend to grow as $O(n^2)$, where n is the number of unknowns. The time required for solving the system of equations increases as well. These fast-growing complexities end up quickly to make integral methods unfeasible if special techniques are not employed.

Numerical compression techniques such as the Fast Multipole Method (GREENGARD; ROKHLIN, 1987) are available to mitigate these difficulties linked to the increased memory required and the long processing times needed during the integration and assembly steps of integral methods. In the present case, a different numerical scheme is adopted: the inductance matrix $[L]$ is compressed using the $\mathcal{H}$-matrix scheme, and is treated with the Hybrid Cross Approximation (HCA) technique (BÖRM; GRASEDYCK, 2005). A detailed discussion of these numerical procedures is beyond the scope of this work.

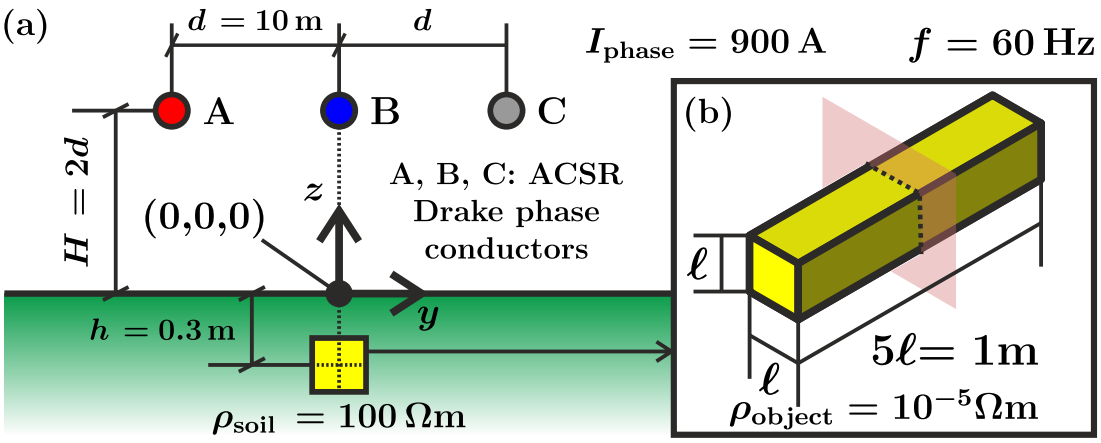

Figure 28: The transmission line right of way (a) and the conductive object underground (b).

5.3 Application to the analysis of inductive couplings with overhead lines

The basic generalized PEEC procedure requires adaptations for treating inductive coupling phenomena in the vicinities of an overhead line.

The need for these adaptations will become clearer in this section, in which a specific problem of application will be described. This description will be followed by a discussion of the modifications carried out in the basic numerical procedure for this class of applications.

5.3.1 Problem description

The configuration to be analyzed is shown in Figure 28, the right of way of a three-phase transmission line where a conductive object of prismatic shape is buried under the soil surface. Its phase conductors A, B and C carry a balanced and symmetrical system of three-phase currents, and the relative position between the line and the object is also shown in the figure. Additional relevant physical information is available in Figure 28 as well.

The aim is to determine the current density distribution in the buried object,

which is induced by the proximity with the overhead line. The problem depicted in Figure 28 will be considered in two conditions. First, the longest dimension of the buried object will be placed in parallel to the overhead line. In a second analysis, the object will be rotated and positioned with its largest dimension orthogonal to the overhead line.

A discussion about the solutions for this problem will be resumed in section 5.4. The adaptations introduced in the PEEC approach to handle inductive coupling situations involving transmission lines will be now outlined.

5.3.2 Adaptations on the basic procedure

The application of the PEEC formulation presented in section 5.2 to the problem under analysis would require the inclusion of the three phase line conductors into conductive region Ω, together with the soil and the object buried in the right of way. As a consequence, their volume discretization with facet elements would be required as well. This modeling alternative would result in a large number of additional degrees of freedom (or unknown facet currents) in the system of equation, leading to problems of intractable sizes, according to the discussion contained in section 5.2.5.

An alternative approach is proposed to avoid this, involving the consideration of two separate conductive regions. Figure 29 displays the decomposition of Ω into two sub-regions. The first corresponds to a sufficiently large soil volume Ω_V, bounded by the earth surface and including the embedded underground object. In Ω_V, $\mathbf{J}$ is approximated by vector facet elements as described in section 5.2.2, which can be associated to a space $\{\mathbf{v}_i\}$ of vector facet functions.

The second sub-region is given by transmission line Ω_L, which is modeled

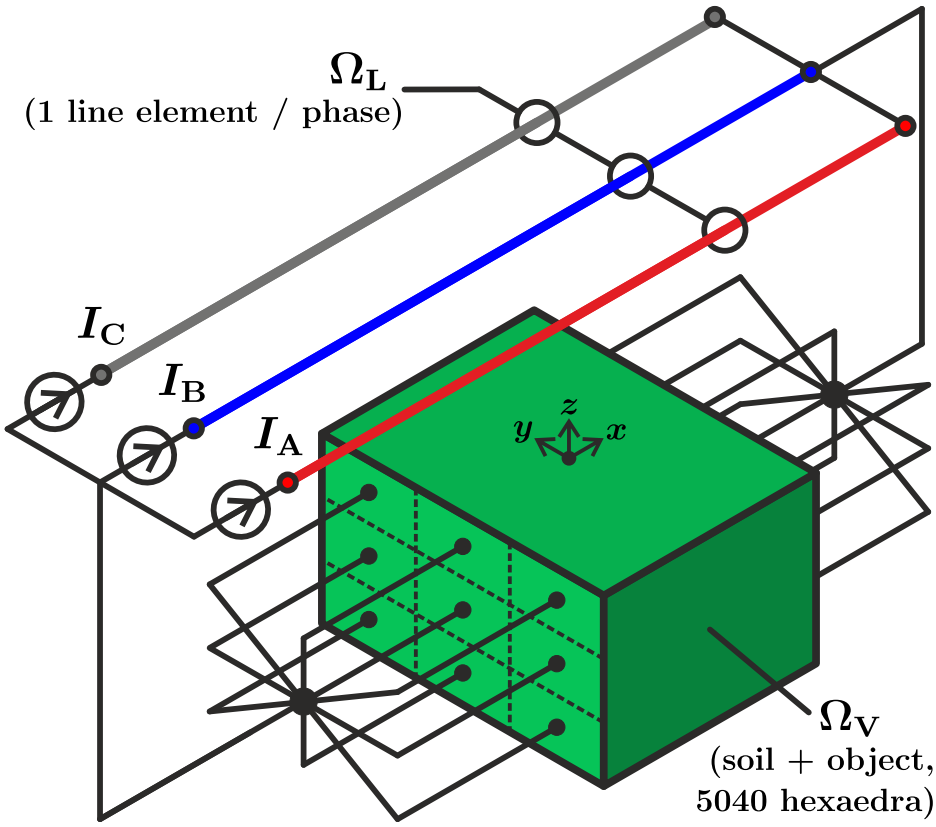

Figure 29: The computational domain and its connections to the external circuit. The conductive object shown in Figure 28 is embedded inside the green box of soil.

by line elements, each carrying a constant complex current and with one single long element per phase conductor. This corresponds to adopting a space of zero order interpolation functions $\{\mathbf{u}_i\}$ with a pre-defined direction for describing the current distribution in Ω_L, thereby limiting the number of additional degrees of freedom.

This procedure may be formally regarded as a coupling between the generalized PEEC method (applied to the soil and the buried object) and the classical PEEC method (applied to the transmission line), as described in (NGUYEN, 2014).

With two different function spaces $\{\mathbf{v}_i\}$ and $\{\mathbf{u}_i\}$ for approximating the current density distribution in $\Omega = \Omega_V \cup \Omega_L$, the assembly of the terms (5.10) into (5.9) yields a system matrix partitioned into four blocks, as shown in Figure 30.

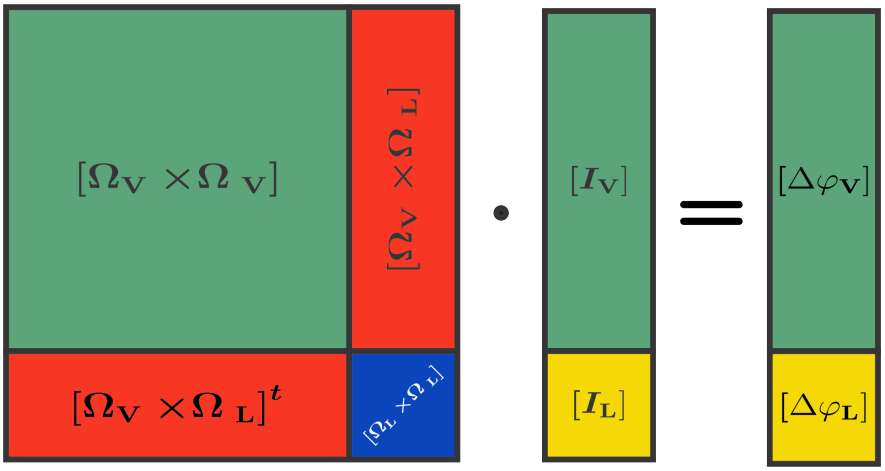

Figure 30: Topology of the algebraic system of equations yielded by the modified PEEC formulation to the domain of Figure 29, showing a 4-block partitioning structure.

The terms to be assembled to the global system of equations are still given by (5.10), but with the additional remark that now $\{\mathbf{w}_i\} = \{\mathbf{v}_i\} \cup \{\mathbf{u}_i\}$.

The large matrix block $[\Omega_V \times \Omega_V]$ corresponds to the soil and object interactions. Therefore, its general terms become:

$$R_{ij} = \int_{\Omega} \frac{\mathbf{v}_i \cdot \mathbf{v}_j}{\sigma} \, \mathrm{d}\Omega \,, \tag{5.11a}$$

$$L_{ij} = \frac{\mu_0}{4\pi} \int_{\Omega} \mathbf{v}_i \cdot \left(\int_{\Omega} \frac{\mathbf{v}_j}{r} \, \mathrm{d}\Omega \right) \mathrm{d}\Omega. \tag{5.11b}$$

The sparsity properties of the resistive and inductive parts addressed in section 5.2.5 remain valid for this block. Thus, (5.11b) leads to a dense matrix, thereby requiring matrix compression.

Blocks $[\Omega_V \times \Omega_L]$ and $[\Omega_V \times \Omega_L]^t$ are associated to the interactions between the overhead line and the ensemble composed by the soil and its buried object. Only the computation of one of this blocks needs to be actually carried out, since the other one may be obtained by matrix transposition. The general

terms of $[\Omega_V \times \Omega_L]$, are then given by:

$$R_{ij} = \int_{\Omega} \frac{\mathbf{v}_i \cdot \mathbf{u}_j}{\sigma} \, d\Omega = 0, \tag{5.12a}$$

$$L_{ij} = \frac{\mu_0}{4\pi} \int_{\Omega} \mathbf{v}_i \cdot \left(\int_{\Omega} \frac{\mathbf{u}_j}{r} \, d\Omega \right) d\Omega. \tag{5.12b}$$

The last block $[\Omega_L \times \Omega_L]$ is associated to the interactions involving only the phase conductors of the overhead line. The block may be promptly identified with the line impedance matrix, containing the phase conductors self--impedances in its main diagonal and the mutual impedances between phases in the other positions.

For the line shown in Figure 28, this block is reduced to a small 3×3 matrix that is particularly prone to the numerical integration difficulties discussed in section 5.2.5, which were related to the evaluation of a singular integrand during the Gaussian quadrature. Therefore, this last block is not integrated numerically, but is instead substituted by an analytical computation of the three-phase line impedance matrix. Details on the analytical computation of the impedance matrix of an overhead line are widely available in reference manuals (LAFOREST, 1982) or in power engineering textbooks (STEVENSON, 1982).

Figure 29 also shows a three-phase source providing current excitation and the circuit interconnection between Ω_V and Ω_L. This external network is introduced and treated only at the level of the electric circuit solver employed for the solution. This possibility was previously quoted as one of the motivations for adopting the circuit solver approach for the solution of the system of equations.

Note that the interconnections linking Ω_V and Ω_L establish an underground path for the flow of zero-sequence current components (if an unbalanced operation condition is to be considered). The remaining facets on the boundary of

Ω_V not linked to the external circuit are subjected to a homogeneous Dirichlet boundary condition (that is, null facet currents).

5.4 Application and Results

The application of the adapted PEEC approach was carried out for two configurations of the problem of Figure 28, namely two different alignments between the three-phase line and the object.

The difference between these two variants stands in their possibilities of being analyzed by an alternate 2-D model. The case in which the object is placed in parallel to the overhead line belongs to a category of applications that can be somehow reduced to a representative 2-D problem, while the orthogonal variant does not.

Consequently, the 3-D PEEC solution of the former will be confronted with the one issued from a simple and straightforward 2-D FEM approach. On the other hand, the validation of the 3-D PEEC solution of the latter will be accomplished with the aid of a full 3-D FEM model that suffers from some of the complications listed in section 5.1.

For analyzing both cases with the generalized PEEC approach, structured meshes of 5040 hexahedra were adopted for discretizing Ω_V. Similarly, the complete equivalent network arising from the PEEC numerical scheme for each configuration had approximately 15000 branches and 9500 independent current loops.

The 2-D and 3-D FEM computations adopted as benchmarks were performed with the commercial FLUX software package (CEDRAT, 2015). The implementation of the PEEC software tool was accomplished with the aid of MIPSE, a Java library developed in G2ELAB (*Laboratoire de Génie Électrique*

de Grenoble).

A detailed discussion on the two problems analyzed is given as follows. For both cases, the efforts are concentrated on demonstrating the relative accuracy of the PEEC approach in comparison with the FEM.

5.4.1 Parallel alignment and 2-D FEM validation

Provided that the length of the buried object ($5\ell = 1\,\mathrm{m}$) is several times longer than its other dimensions ($\ell = 0.2\,\mathrm{m}$) and that its parallel alignment with respect to the overhead line is considered, the PEEC solution obtained in the mid-section of the buried object may be compared with a 2-D FEM computation.

The referred mid-section is highlighted in Figure 28(b), and the 2-D finite element solution assumes a buried object of infinite length and current density $\mathbf{J}$ parallel to the transmission line. Notwithstanding these assumptions, the interest in adopting a 2-D FEM computation as a benchmark lies in the possibility of employing very fine discretization meshes while keeping the problem tractable from a numerical point of view, which ultimately leads to accurate solutions.

Therefore, a magnetodynamic finite element simulation was carried out with a very fine mesh of second order triangular elements, as seen in Figure 31(a). The current density yielded by this approach is given in Figure 31(b).

A profile of the structured mesh of hexahedra utilized in the 3-D PEEC computations is shown in Figure 31(c). It should be noticed that this mesh is much coarser when compared to the one employed in the 2-D finite element simulation. This difference in the discretization approach is due to the peculiarities of the PEEC method discussed in section 5.2.5, which easily make the treatment of problems with a larger number of degrees of freedom unpractical in terms of

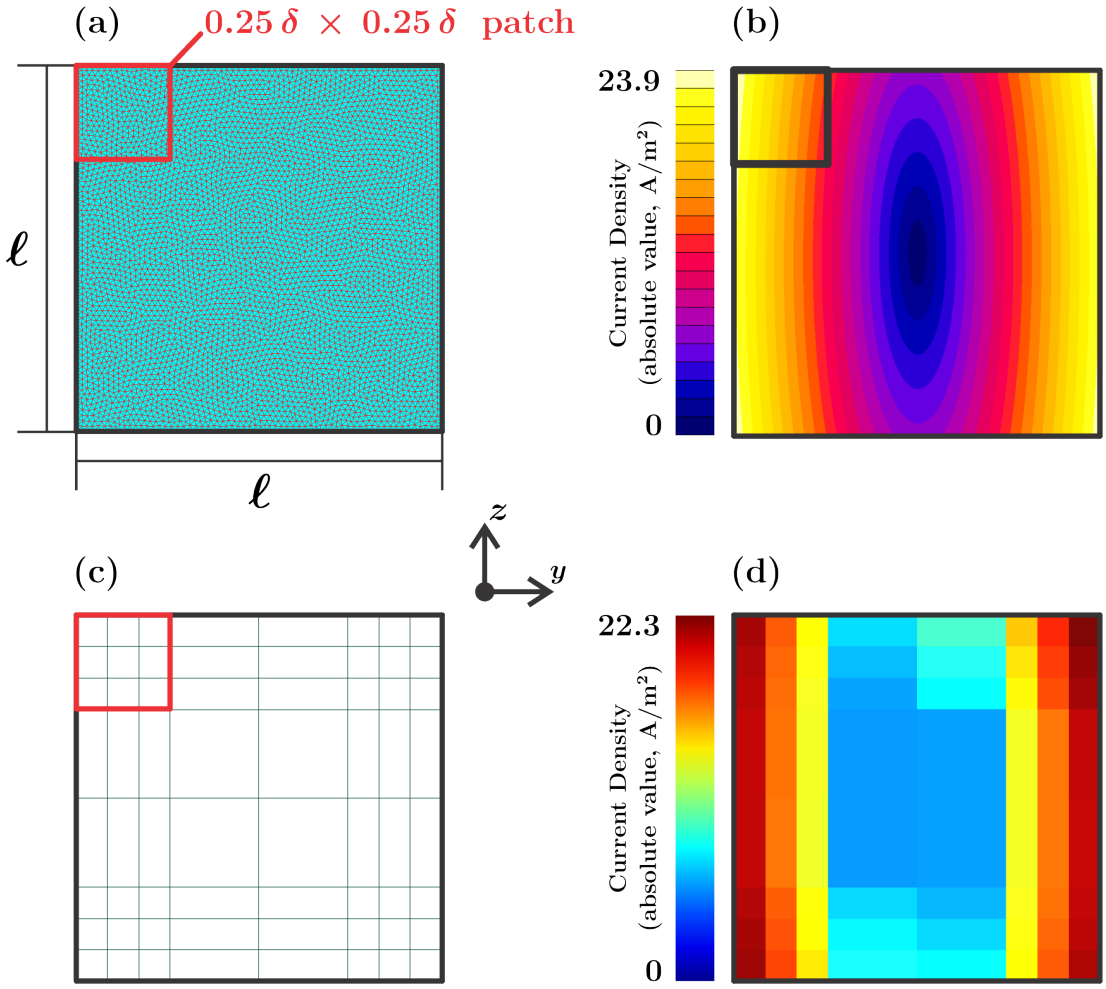

Figure 31: Comparison of the discretization meshes and of the current density distributions in the mid-section of the buried object for the 2-D FEM and the 3-D generalized PEEC method.

storage capacity and computation time.

A cut of the buried object through its mid-section with the current density issued from the PEEC solution is also shown in Figure 29(d). A quantitative comparison between this solution and its 2-D FEM counterpart shown in Figure 29(d) may be carried out in terms of two quantities, namely, the magnitude of the current density distribution in the object cross-section and its mean value.

The support for the computation of the mean value was arbitrarily chosen as a square patch located in the corner of the object cross-section, as shown

Table 3: PEEC and 2-D FEM Comparison (parallel case)

	2-D FEM	PEEC	% Deviation*
$\|\mathbf{J}\|_{max}$ †	23.9	22.3	6.7
$\|\mathbf{J}\|_{mean}$ ‡	17.8	17.4	2.2

† Maximum current density in the object cross-section ($\mathrm{A/m^2}$).
‡ Computed in the left upper corner patch shown in Figure 31 ($\mathrm{A/m^2}$) .
* Between the PEEC value and the reference 2-D FEM solution.

in Figure 31. This patch is dimensioned in terms of skin-depth δ of the electromagnetic fields inside the buried object, namely about 0.205 m in the case treated.

Table 3 gives the values assumed by these quantities. The percent deviations of the PEEC solutions with respect to the 2-D finite element values are available in this table as well. The analysis of these deviations shows that a good agreement between the maximum current density $|\mathbf{J}|_{max}$ computed with the two different approaches was verified, and an even better accord was obtained for the average values $|\mathbf{J}|_{mean}$ evaluated over the highlighted $0.25\,\delta \times 0.25\,\delta$ patch.

5.4.2 Orthogonal alignment and 3-D FEM validation

The second test case corresponds to the line and the object in an orthogonal alignment. The resulting configuration can be handled by the PEEC technique as before, but the obtained current density distribution inside the object is no longer comparable with the one issued from a 2-D finite element computation.

The spatial distribution of $\mathbf{J}$ inside the object resulting from the coupling with the three-phase line and computed with the PEEC approach is shown in Figure 32. Figure 33 brings a somewhat more quantitative view of the eddy current loops established inside the object by showing the absolute value of

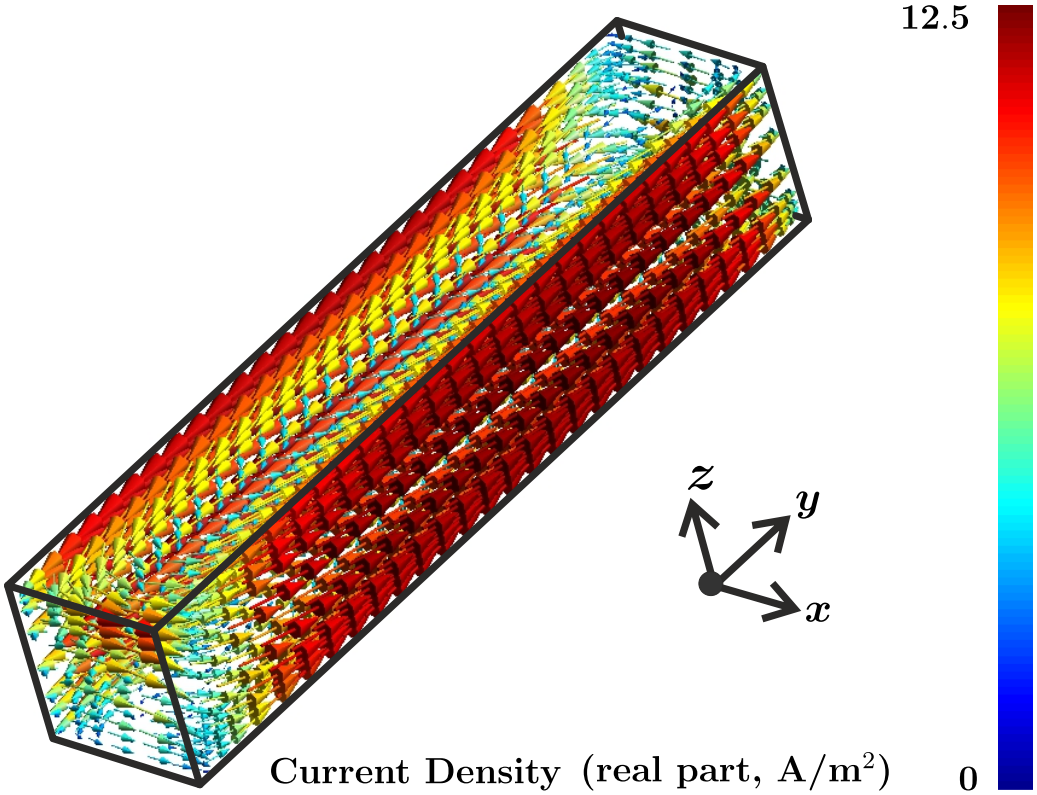

Figure 32: Spatial distribution of the induced current density.

each component of $\mathbf{J}$ in its horizontal mid-section ($z = -0.3\,\mathrm{m}$).

The 3-D finite element solution for the problem corresponding to the orthogonal orientation is computationally demanding. A $\mathbf{t} - \mathbf{t_0} - \phi$, circuit-coupled formulation (MEUNIER; FLOCH; GUERIN, 2003; FLOCH et al., 2003) was employed with a similar structured mesh of hexahedra as in the PEEC case, with the remark that the FEM cannot avoid the discretization of the air regions.

With this method, the determination of an induced current distribution in the buried object that remains insensitive to additional refinements in the discretization requires a very dense mesh of hexahedra, long computation times and a large memory capacity. However, the maximum current density value inside the object may be approximated by an asymptotic value of approximately $21.85\,\mathrm{A/m^2}$. This limiting value is obtained by the 3-D FEM computation of the maximum current density for a series of increasingly refined meshes and by

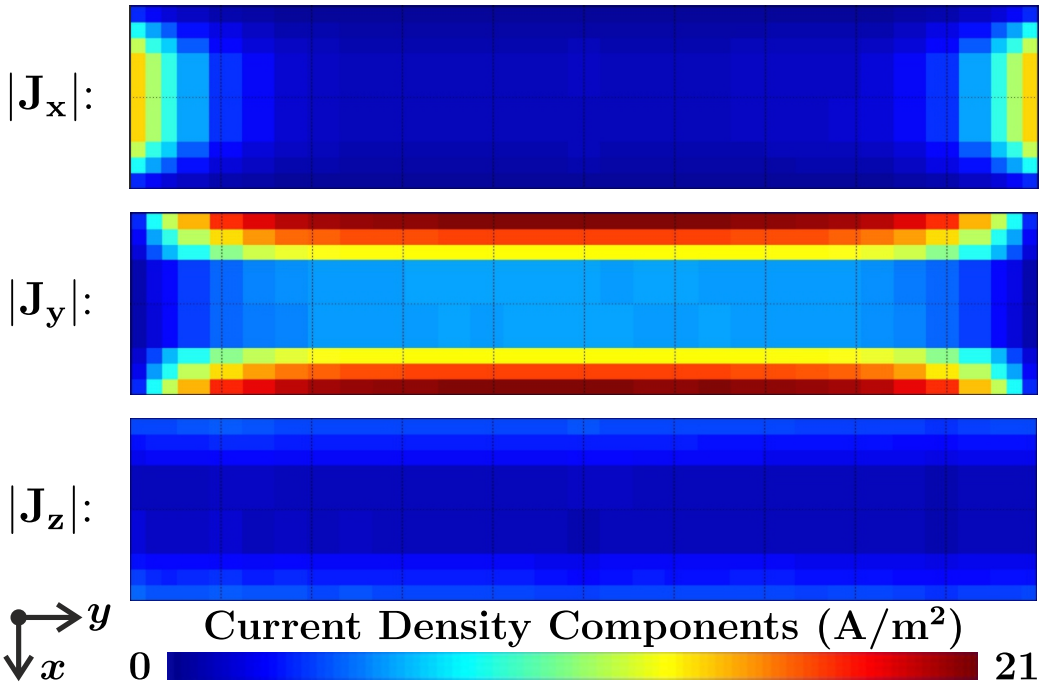

Figure 33: Current density in the horizontal mid-section of the buried object.

extrapolation, as implied by Figure 34.

If this value $|\mathbf{J}|_{\text{max}} = 21.85\,\text{A/m}^2$ is fixed as a reference, the maximum current densities computed with the PEEC scheme and the 3-D FEM may be com-

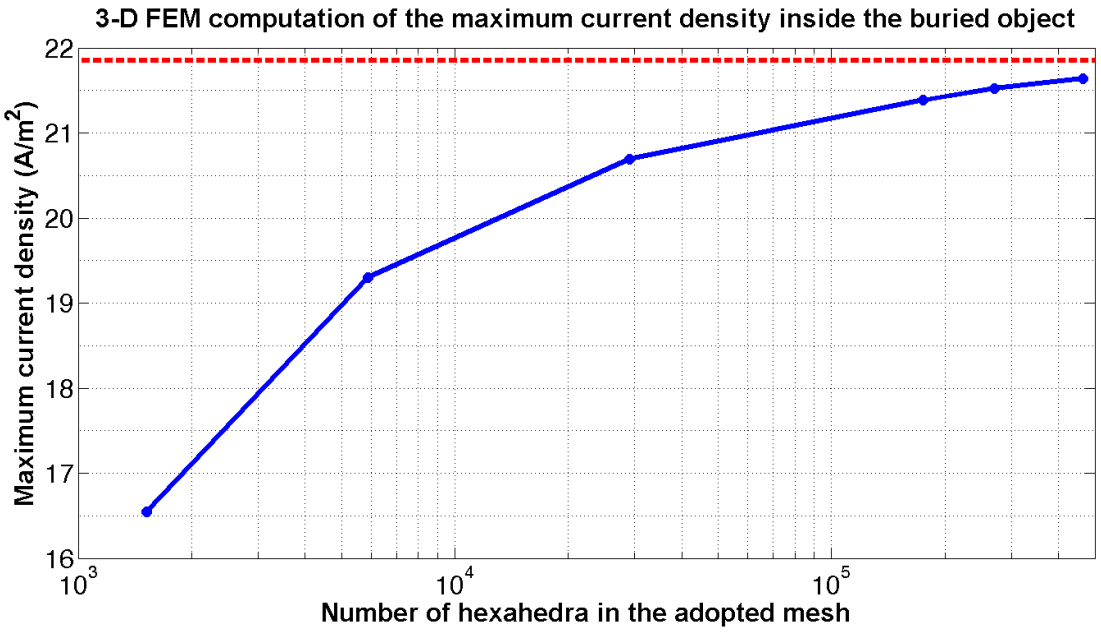

Figure 34: Determination of the asymptotic value of the maximum current density inside the buried object with the 3D-FEM (orthogonal case).

Table 4: PEEC and 3-D FEM Comparison (orthogonal case)

Method	Mesh size†	$\|\mathbf{J}\|_{max}$‡	% Deviation
Reference*	-	21.85	0
3-D FEM	5880	19.30	11.67
PEEC	5040	21.20	2.97

† Number of elements in the discretization.
‡ Maximum current density inside buried object ($\mathrm{A/m^2}$).
* Stable solution estimated by Figure 34.

pared. Table 4 provides this comparison between the two procedures when the maximum current density values developed inside the underground object are evaluated with practical and relatively coarse meshes, both containing a similar number of elements (≈ 5000 hexahedra). For a given mesh size, the PEEC approach is verified to be able to provide a more accurate solution than the 3-D FEM.

A systematic performance comparison between the FEM and the generalized PEEC method in this class of applications is left for future works. Even though the PEEC approach was shown to yield more accurate solutions with coarser meshes, in the current state of developments the comparison of computation times still tends to be biased towards the FEM. This is markedly the case when large deviations from the reference value fixed in Figure 34 are admissible.

5.5 Chapter summary

This chapter presented an approach based on the generalized PEEC method for analyzing inductive coupling phenomena involving an overhead power line and an underground conductive object. Two relative positions between the transmission line and the object have been considered, and the current density distribution developed in the object was determined in each case.

The current density distribution obtained could provide base data for the study of AC corrosion phenomena (REVIE, 2015; CENELEC, 2013). Moreover, the electric potential solution in the domain Ω resulting from the circuit equivalence discussed in section 5.2.4 could also be conveniently employed to evaluate dangerous induced overvoltages.

The solutions computed with the generalized PEEC approach were validated by comparison with 2-D and 3-D FEM models and accurate solutions (i.e a small percent deviation from finite element analysis) were obtained with the use of the PEEC approach. In face of these results, extensions of the basic procedure could be envisaged. For instance, the use of more complex external networks could be exploited in the investigation of other practical problems arising in power engineering, such as the occurrence of a simultaneous fault to earth in the three-phase line. The account of capacitive effects could be introduced at the level of the external network as well, leading to interesting model possibilities that would only became feasible in the context of the FEM with the use of other formulations.

As quoted in section 5.4.2, a systematic performance comparison between the generalized PEEC approach and the FEM is still to be made for this application. Future works on numerical aspects such as improved integration procedures, system assembly techniques and matrix pre-conditioning could be envisioned and are expected to result in significant gains in performance.

It should still be remarked that the problems of application of in this chapter considered only the case of a balanced system of three-phase currents flowing in the phase conductors of the transmission line. Further work on this subject also intends to investigate the case of unbalanced operation and the consequent superposition of conductive coupling phenomena, resulting from the flow of zero-sequence current components in the soil.

6 CONCLUSIONS AND PERSPECTIVES

6.1 General remarks

In the previous chapters, the numerical modeling of electromagnetic coupling phenomena resulting from the proximity with overhead power transmission lines has been addressed. Conductive and inductive phenomena were modeled respectively with the Finite Element Method and with the generalized Partial Element Equivalent Circuit Method. Additionally, problems of application were considered in both cases.

The analyses of these two categories of applications were carried out with the apparently restrictive assumption of a single and homogeneous resistivity for the soil. Moreover, the boundary condition scheme proposed for truncating the domain in conductive coupling applications even relies on this hypothesis, as seen in chapter 3.

In the discussion whether or not this approach provides an adequate representation of the soil, it should be remarked that the actual soil properties are influenced by a broad range of factors such as moisture content, amount of dissolved salts, grain size and distribution, temperature, season of the year, etc. This particular behavior turns the accurate modeling of the soil into a complex and frequently unfruitful effort.

As a consequence, in the practice of power engineering, complex soil mod-

els for real situations are often unavailable. On the other hand, the direct determination of a single and apparent resistivity of the soil is a simple and straightforward procedure. Typical values are also readily available for the most common soil types. In this sense, the use of single-valued, homogeneous resistivity model imposes itself from a practical point of view, relaxing that apparent constraint.

Nevertheless, the use of more elaborate soil models could be considered. For instance, the use of a multilayered soil model in the inductive coupling applications of chapter 5 is only a simple matter of representing the various strata of soil in the computational domain. In the case of the conductive coupling applications of chapter 4, an additional modification of (3.21) computing the boundary condition on the electric potential would have to be considered as well, and the results provided by (STEFANESCO; SCHLUMBERGER; SCHLUMBERGER, 1930) could be considered for this purpose.

Additional improvements or extensions to other modeling aspects proposed in this work could be envisioned in a similar way. The investigation of electromagnetic coupling phenomena in transmission line rights of ways is a broad field of inquiry, and not surprisingly this subject could not be exhausted in this work. This said, the following sections are devoted to recalling the main achievements obtained with this thesis and to accounting new endeavors that could follow from the current state of developments in this domain.

6.2 Contributions of this work

The developments achieved in the course of this work converge on providing means of simulating general coupling situations occurring in the vicinities of an overhead line.

The following main contributions could be highlighted among them:

- A special boundary condition for finite element formulations based on the approximation of the electric scalar potential was proposed to address the truncation of the computational domain. The numerical scheme allows considering multiple sources of current injection into the soil, as required in the investigation of complex conductive coupling situations taking place in a right of way.

- The conditions of applicability of this boundary condition technique were verified and shown to be related to the adequate dimensioning of the computational domain and to the conductive character of buried heterogeneities. The scope of application was verified to be wide enough to allow investigating real problems in power engineering, as shown in section 4.6.

- The modeling of inductive coupling phenomena with the generalized PEEC method was proposed. The results from this approach were shown to be in accordance with a well-established finite element models even when relatively coarse meshes are employed.

- The choice of this integral method and its coupling with the classical PEEC method avoided discretizing both inactive air regions and thin phase conductors of the overhead line, which are recognized complications in the development of full 3-D models in computational electromagnetics.

- A direct and simplified interface with external circuits was provided by the choice of a PEEC-based approach for modeling inductive coupling phenomena, giving rise to the possibility of integrating the 3-D model of

a particular right of way with network analysis tools representing large scale power systems.

6.3 Topics for later development

The following topics are suggestions for later developments and could be considered for continuing the research carried out:

- Incorporation of other soil models in the finite element modeling of conductive coupling problems (multilayered soils, account of soil ionization).
- Consideration of fast transient fault currents in conductive coupling phenomena and time-domain simulation.
- Improving material modeling both in conductive and inductive coupling applications, allowing the consideration of structures or devices with an arbitrary composition in proximity with an overhead line.
- Enhancing the performance of the simulations based on the generalized PEEC method by means of improved matrix compression techniques, numerical integration procedures and matrix solvers.
- Comparison and validation of the results with measures issued from dedicated experimental arrangements in both conductive and inductive coupling applications.
- Investigation of capacitive coupling problems or of capacitive effects either by the introduction of capacitances in the external PEEC circuit or by the use of an extended PEEC formulation.
- Simultaneous modeling of both conductive and inductive coupling phenomena in a single simulation.

- Modeling inductive coupling problems with alternative integral methods such as the Boundary Element Method coupled with external circuits.
- Investigation of inductive coupling problems involving transmission lines operating in unbalanced conditions, leading to the flow of zero-sequence current components in the soil.

REFERENCES

ANTONINI, G.; CRISTINA, S.; ORLANDI, A. PEEC modeling of high voltage towers under direct and nearby lightning strike. In: *Proceedings of the 10th International Symposium on High Voltage Engineering*. Montréal, Canada: ISH'97, 1997. v. 5, p. 187–203.

BÁRDI, I.; BÍRÓ, O.; PREIS, K. Perfectly matched layers in static fields. *IEEE Trans. Magn.*, v. 34, n. 5, p. 2433–2436, Sept 1998. ISSN 0018-9464.

BERENGER, J.-P. A perfectly matched layer for the absorption of electromagnetic waves. *Journal of Computational Physics*, v. 114, n. 2, p. 185 – 200, 1994. ISSN 0021-9991. Available from Internet: <http://www.sciencedirect.com/science/article/pii/S0021999184711594>.

BÍRÓ, O. Edge element formulations of eddy current problems. *Computer Methods in Applied Mechanics and Engineering*, v. 169, n. 3-4, p. 391–405, February 1999.

BOLLIGER, A. *Probleme der Potentialtheorie*. Thesis (PhD) — Eidgenössische Technische Hochschule Zürich, 1917. Available from Internet: <http://e-collection.library.ethz.ch/view/eth:21149>.

BÖRM, S.; GRASEDYCK, L. Hybrid cross approximation of integral operators. *Numerische Mathematik*, Springer-Verlag, v. 101, n. 2, p. 221–249, 2005. ISSN 0029-599X. Available from Internet: <http://dx.doi.org/10.1007/s00211-005-0618-1>.

BOSSAVIT, A. Whitney forms: a class of finite elements for three-dimensional computations in electromagnetism. *Physical Science, Measurement and Instrumentation, Management and Education - Reviews, IEE Proceedings A*, v. 135, n. 8, p. 493–500, November 1988. ISSN 0143-702X.

CARDOSO, J. R. Fem modelling of grounded systems with unbounded approach. *IEEE Transactions on Magnetics*, v. 30, n. 5, p. 2893–2896, Sep 1994. ISSN 0018-9464.

CARSON, J. R. Wave propagation in overhead wires with ground return. *The Bell System Technical Journal*, v. 5, n. 4, p. 539–554, Oct 1926. ISSN 0005-8580.

CEDRAT. *Flux 12.0 - Electromagnetic and thermal finite element analysis software package*. 2015. Available from Internet: <http://www.cedrat.com/ ; visited on 28 June 2015.>.

CENELEC. *EN 50443 - Effects of electromagnetic interference on pipelines caused by high voltage a.c. electric traction systems and/or high voltage a.c. power supply systems*. 2012. European standard, Comité Européen de Normalisation Électrotechnique.

____. *EN 15280 - Evaluation of a.c. corrosion likelihood of buried pipelines applicable to cathodically protected pipelines*. 2013. European standard, Comité Européen de Normalisation Électrotechnique.

CHOW, Y. L.; YANG, J. J.; SRIVASTAVA, K. D. Complex images of a ground electrode in layered soils. *Journal of Applied Physics*, v. 71, n. 2, p. 569–574, 1992. ISSN 00218979. Available from Internet: <http://scitation.aip.org/content/aip/journal/jap/71/2/10.1063/1.350407>.

CHRISTOFORIDIS, G.; LABRIDIS, D.; DOKOPOULOS, P. Inductive interference on pipelines buried in multilayer soil due to magnetic fields from nearby faulted power lines. *Electromagnetic Compatibility, IEEE Transactions on*, v. 47, n. 2, p. 254–262, May 2005. ISSN 0018-9375.

CIGRÉ. *Guide on the influence of high voltage AC power systems on metallic pipelines*. Paris, France, 1995. Conseil International des Grands Réseaux Électriques, Working Group 36.02. Available from Internet: <http://e-cigre.org>.

DALZIEL, C. F. Effects of electric shock on man. *IRE Transactions on Medical Electronics*, PGME-5, p. 44–62, July 1956. ISSN 0097-1049.

DAWALIBI, F. Ground fault current distribution between soil and neutral conductors. *IEEE Transactions on Power Apparatus and Systems*, PAS-99, n. 2, p. 452–461, March 1980. ISSN 0018-9510.

DAWALIBI, F.; BENSTED, D.; MUKHEDKAR, D. Soil effects on ground fault currents. *IEEE Trans. Power App. Syst.*, PAS-100, n. 7, p. 3442–3450, July 1981. ISSN 0018-9510.

DAWALIBI, F.; MUKHEDKAR, D. Optimum design of substation grounding in a two layer earth structure: Part I - Analytical study. *IEEE Transactions on Power Apparatus and Systems*, v. 94, n. 2, p. 252–261, Mar 1975. ISSN 0018-9510.

DAWALIBI, F.; SOUTHEY, R. Analysis of electrical interference from power lines to gas pipelines. I. Computation methods. *Power Delivery, IEEE Transactions on*, v. 4, n. 3, p. 1840–1846, Jul 1989. ISSN 0885-8977.

DAWALIBI, F. et al. *Power Line Fault Current Coupling to Nearby Natural Gas Pipelines*. Houston, Texas, October 1988. Pipeline Research Council International (PRCI). Project Number PR-151-634, Catalog Number L51537. Available from Internet: <http://prci.org>.

DHATT, G.; TOUZOT, G.; LEFRANÇOIS, E. *Méthode des éléments finis*. Paris: Lavoisier, 2007.

DULAR, P. et al. Mixed finite elements associated with a collection of tetrahedra, hexahedra and prisms. *IEEE Trans. Magn.*, v. 30, n. 5, p. 2980–2983, Sept 1994. ISSN 0018-9464.

FAVEZ, B.; GOUGEUIL, J. Contribution to studies on problems resulting from the proximity of overhead lines with underground metal pipe lines. *CIGRE paper*, n. 336, 1966.

FILHO, M. L. P.; CARDOSO, J. R. Modelling of ground grids in multilayer soils using complex images. In: *Proceedings of the 12th International Conference on the Computation of Electromagnetic Fields - COMPUMAG 1999*. Sapporo, Japan: International Compumag Society, 1999. v. 2, p. 782–783.

FLOCH, Y. L. et al. Coupled problem computation of 3-d multiply connected magnetic circuits and electrical circuits. *Magnetics, IEEE Transactions on*, v. 39, n. 3, p. 1725–1728, May 2003. ISSN 0018-9464.

FRAZIER, M. *Power Line-Induced AC Potential on Natural Gas Pipelines for Complex Rights-of-Way Configurations*. Houston, Texas, May 1984. Pipeline Research Council International (PRCI). Project Number PR-151-127, Catalog Number L51418. Available from Internet: <http://prci.org>.

GREENGARD, L.; ROKHLIN, V. A fast algorithm for particle simulations. *Journal of Computational Physics*, v. 73, n. 2, p. 325 – 348, 1987. ISSN 0021-9991. Available from Internet: <http://www.sciencedirect.com/science/article/pii/0021999187901409>.

JACKSON, J. D. *Classical Electrodynamics*. 3rd. ed. Hoboken, NJ: John Wiley & Sons, Inc., 1999.

LAFOREST, J. J. *Transmission Line Reference Book - 345 kV and Above*. 2nd. ed. Palo Alto, CA: Electric Power Research Institute, 1982.

MARTINHO, L.; SILVA, V. Effects of external currents and soil heterogeneities on an approximate boundary condition for the 3-D finite element analysis of subsurface conductive coupling problems. *IEEE Trans. Magn.*, v. 51, n. 3, p. 1–4, March 2015. ISSN 0018-9464.

MARTINHO, L. et al. 3-D finite-element analysis of conductive coupling problems in transmission line rights of way. *IEEE Trans. Magn.*, v. 50, n. 2, p. 969–972, Feb 2014. ISSN 0018-9464.

____. A non-homogeneous Dirichlet boundary condition on the electric potential for the finite element analysis of grounding systems. In: *Proceedings of the 8th IET International Conference on Computation in Electromagnetics (CEM 2011)*. Wrocław, Poland: Institution of Engineering and Technology, 2011. p. 104–105.

MEUNIER, G.; FLOCH, Y. L.; GUERIN, C. A nonlinear circuit coupled t-t0- phi; formulation for solid conductors. *Magnetics, IEEE Transactions on*, v. 39, n. 3, p. 1729–1732, May 2003. ISSN 0018-9464.

NEKHOUL, B. et al. A finite element method for calculating the electromagnetic fields generated by substation grounding systems. *Magnetics, IEEE Transactions on*, v. 31, n. 3, p. 2150–2153, May 1995. ISSN 0018-9464.

____. Calculating the impedance of a grounding system. *IEEE Transactions on Magnetics*, v. 32, n. 3, p. 1509–1512, May 1996. ISSN 0018-9464.

NGUYEN, T.-S. et al. An independent loops search algorithm for solving inductive PEEC large problems. *Progress In Electromagnetics Research M*, v. 23, p. 53–63, 2012.

NGUYEN, T. T. *Méthode PEEC inductive par élément de facette pour la modélisation des régions conductrices volumiques et minces*. Thesis (PhD) — Université de Grenoble, out. 2014. In French. Available from Internet: <https://hal.archives-ouvertes.fr/tel-01115779 ; visited on 28 June 2015.>.

NGUYEN, T.-T. et al. An integral formulation for the computation of 3-D eddy current using facet elements. *Magnetics, IEEE Transactions on*, v. 50, n. 2, p. 549–552, Feb 2014. ISSN 0018-9464.

OLLENDORFF, F. Der Stromübergang aus langgestreckten Leitern in die Erde. *Wissenschaftliche Veröffentlichungen aus dem Siemens-Konzern*, v. 5, n. 3, p. 8–28, October 1926.

____. *Erdströme - Grundlagen der Erdschluss und Erdungsfragen*. Berlin: Julius Springer Verlag, 1928.

POHL, J. Influence of high-voltage overhead lines on covered pipelines. *CIGRE Paper*, n. 326, p. 1090–1097, 1966.

POLLACZEK, F. Über das Feld einer unendlich langen wechselstromdurchflossenen Einfachleitung. *Elektrische Nachrichtentechnik*, v. 3, n. 9, p. 339–359, Sept 1926. French translation also available in *Revue Générale de l'Électricité*, v. 29, n. 22, p. 851-867, May 1931.

____. Sur le champ produit par un conducteur simple infiniment long parcouru par un courant alternatif. *Revue Générale de l'Électricité*, v. 29, n. 22, p. 851–867, May 1931. Original article in german available in *Elektrische Nachrichtentechnik*, v. 3, n. 9, p. 339-359, Sept 1926.

REVIE, R. W. *Oil and Gas Pipelines Integrity and Safety Handbook*. 1st. ed. Hoboken, NJ: John Wiley & Sons, Inc., 2015.

RÜDENBERG, R. Grounding principles and practice I - fundamental considerations on ground currents. *Electrical Engineering*, v. 64, n. 1, p. 1–13, Jan 1945. ISSN 0095-9197.

RUEHLI, A. E. Equivalent circuit models for three-dimensional multiconductor systems. *IEEE Transactions on Microwave Theory and Techniques*, v. 22, n. 3, p. 216–221, Mar 1974. ISSN 0018-9480.

SATSIOS, K.; LABRIDIS, D.; DOKOPOULOS, P. Finite element computation of field and eddy currents of a system consisting of a power transmission line above conductors buried in nonhomogeneous earth. *IEEE Transactions on Power Delivery*, v. 13, n. 3, p. 876–882, Jul 1998. ISSN 0885-8977.

SEBŐ, I.; RÉGENI, L. Measurement of the zero-sequence current distribution on a transmission line. *Periodica Polytechnica*, v. 7, n. 7, p. 295–317, 1963.

SES. *CDEGS - Current Distribution, Electromagnetic Fields, Grounding and Soil Structure Analysis software package by Safe Engineering Services & Technologies Ltd.* 2015. Available from Internet: <http://www.sestech.com/ ; visited on 02 December 2015.>.

SILVA, V. et al. Determination of frequency-dependent characteristics of substation grounding systems by vector finite-element analysis. *IEEE Trans. Magn.*, v. 43, n. 4, p. 1825–1828, April 2007. ISSN 0018-9464.

____. Efficient modeling of thin wires in a lossy medium by finite elements applied to grounding systems. *IEEE Trans. Magn.*, v. 47, n. 5, p. 966–969, May 2011. ISSN 0018-9464.

SILVA, V. C. *Método de elementos finitos aplicado à solução de problemas de aterramento elétrico*. Thesis (Livre Docência) — Escola Politécnica da Universidade de São Paulo, 2006. In Portuguese. Available from Internet: <http://www.teses.usp.br/teses/disponiveis/livredocencia/3/tde-07022007-144705/>.

SILVESTER, P. A general high-order finite-element analysis program waveguide. *IEEE Transactions on Microwave Theory and Techniques*, v. 17, n. 4, p. 204–210, Apr 1969. ISSN 0018-9480.

SILVESTER, P.; CHARI, M. Finite element solution of saturable magnetic field problems. *IEEE Transactions on Power Apparatus and Systems*, PAS-89, n. 7, p. 1642–1651, Sept 1970. ISSN 0018-9510.

SOBRAL, S. et al. Interferences between faulted power circuits and communication circuits or pipelines - Simplification using the decoupled method. *IEEE Transactions on Power Delivery*, v. 6, n. 4, p. 1599–1606, Oct 1991. ISSN 0885-8977.

STEFANESCO, S.; SCHLUMBERGER, C.; SCHLUMBERGER, M. Sur la distribution électrique potentielle autour d'une prise de terre ponctuelle dans un terrain à couches horizontales, homogènes et isotropes. *Le journal de physique et le radium*, v. 7, n. 1, p. 132–140, 1930.

STEVENSON, W. D. *Elements of Power System Analysis*. 4th. ed. Singapore: McGraw-Hill, 1982.

STOHCHNIOL, A. A general transformation for open boundary finite element method for electromagnetic problems. *IEEE Transactions on Magnetics*, v. 28, n. 2, p. 1679–1681, Mar 1992. ISSN 0018-9464.

STOLL, R.; CHEN, G.; PILLING, N. Comparison of two simple high-frequency earthing electrodes. *IEE Proceedings - Generation, Transmission and Distribution*, v. 151, n. 2, p. 219–224, March 2004. ISSN 1350-2360.

STRATTON, J. A. *Electromagnetic Theory*. Reissue of the 1941 edition. Hoboken, NJ: IEEE Press and John Wiley & Sons, Inc., 2007.

SUNDE, E. D. *Earth conduction effects in transmission systems*. 1st. ed. New York: D. Van Nostrand, 1949.

TRLEP, M.; HAMLER, A.; HRIBERNIK, B. The analysis of complex grounding systems by fem. *IEEE Transactions on Magnetics*, v. 34, n. 5, p. 2521–2524, Sep 1998. ISSN 0018-9464.

YEE, K. Numerical solution of initial boundary value problems involving Maxwell's equations in isotropic media. *IEEE Transactions on Antennas and Propagation*, v. 14, n. 3, p. 302–307, May 1966. ISSN 0018-926X.

YUTTHAGOWITH, P. et al. Application of the partial element equivalent circuit method to analysis of transient potential rises in grounding systems. *IEEE Transactions on Electromagnetic Compatibility*, v. 53, n. 3, p. 726–736, Aug 2011. ISSN 0018-9375.

ZIENKIEWICZ, O. C.; TAYLOR, R. L.; ZHU, J. Z. *The Finite Element Method: Its Basis and Fundamentals*. 6th. ed. Oxford: Elsevier, 2006.